skb.se

SKB P-23-09

ISSN 1651-4416

ID 2013128

September 2023

Prototype Repository

Modelling cation exchange in deposition hole 1

Virginia Cabrera, Ersan Demirer, Emilie Coene, Arnau Pont, Andrés Idiart
Amphos 21 Consulting S.L.

Contents

1 Introduction

1.1 Background

The Prototype Repository field test at Äspö Hard Rock Laboratory is a full-scale experiment simulating conditions relevant for the KBS-3 concept for final disposal of high-level radioactive waste (Figure 1-1). The test is located in the bottom section of the TBM-tunnel at the −450 m level. The project aims to improve the understanding of the hydro-mechanical and chemical behaviour of bentonite buffers at temperatures below 100°C during the water saturation transient. In particular, the objectives of the in-situ test are to test the engineered barriers (buffer, backfill and plugs) and to develop models for predicting and evaluating their functions and performance. The Prototype Repository is a demonstration of the integrated function of the repository and provides a full-scale reference for testing the performance of predictive models.

The layout considers six deposition holes, four in an inner section and two in an outer section. Each deposition hole has a full-scale buffer (rings with a thickness of 35 cm) of compacted bentonite (MX-80) surrounding a copper canister equipped with heaters to simulate the heat generation from the waste. The deposition tunnel is backfilled with a mixture of bentonite and crushed rock (30/70). A massive concrete plug, designed to withstand full water and swelling pressures, separates the test area from the open tunnel system and a second plug separates the two sections. This layout was intended to provide two approximately independent test sections.

The relative humidity, pore pressure, total pressure and temperature in different parts of the test area are monitored. The outer test section (deposition holes 5 and 6) was retrieved during 2010-2011 after approximately eight years of heating and water uptake of the buffer and backfill (Svemar et al. 2016). The monitoring of the inner section has been carried out until now (Goudarzi 2022) and will continue until retrieval.

SKB is planning to open and retrieve the inner section of the in-situ test in 2023 (SKB 2021). Before the start of the operation, the rock mass surrounding the test site was thoroughly characterized and modelled (Rhén and Forsmark 2001). This characterization included the identification of groundwater inflow rates in each deposition hole and the potentially conductive fractures (Figure 1-2).

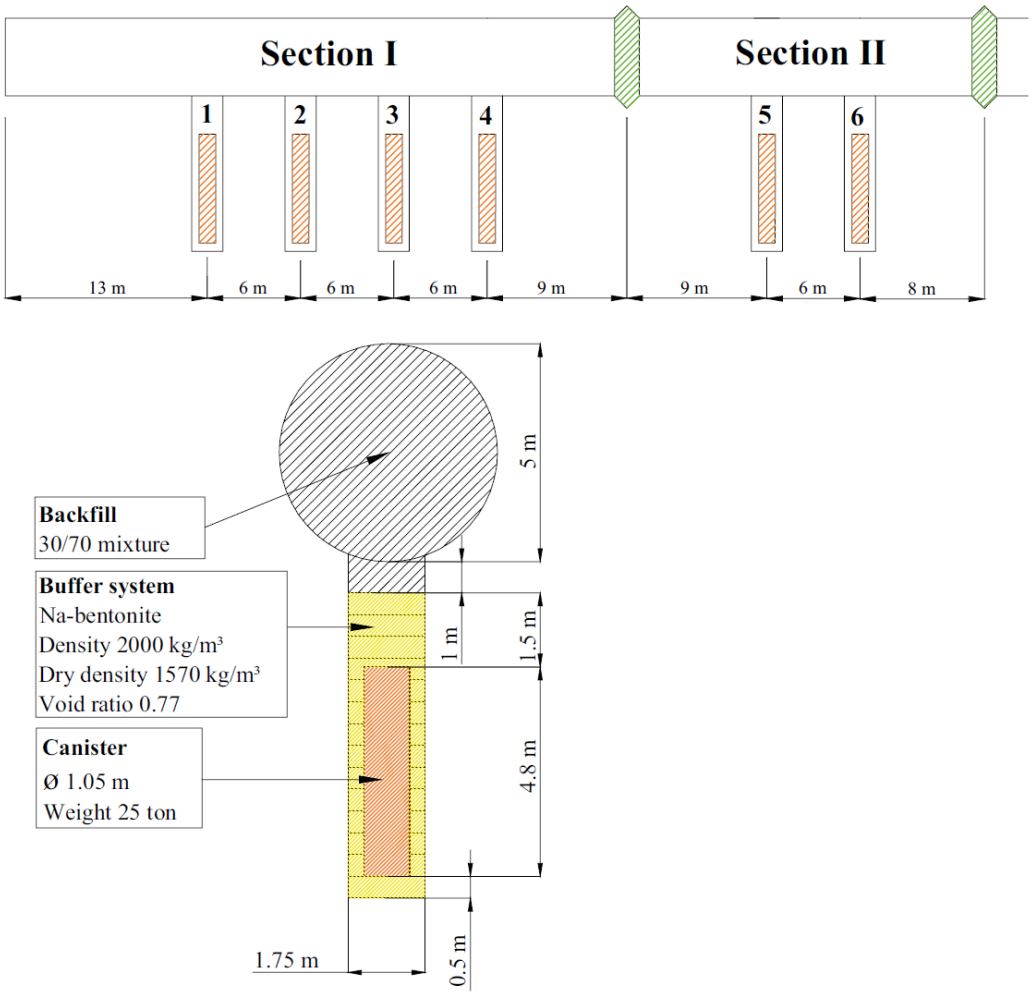

Figure 1-1. *Schematic view of the deposition tunnel (concrete plugs in green) and the deposition holes of the Prototype Repository field test, from Olsson et al. (2013).*

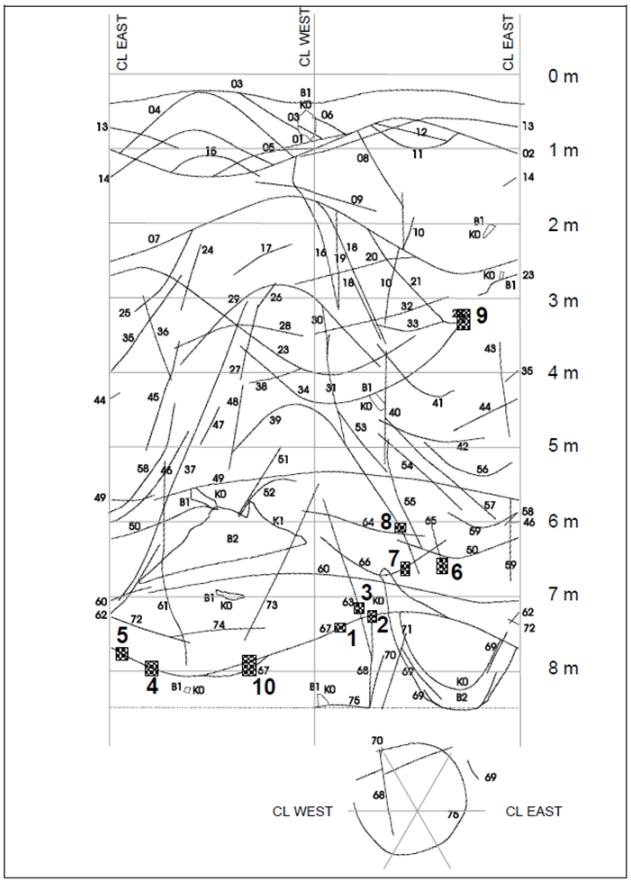

Figure 1-2. *Deposition hole 6 mapping with water-bearing fractures marked with shaded areas (from Rhén and Forsmark 2001).*

1.2 Objectives

The main goal of the project is to assess the groundwater-bentonite interaction in deposition hole number 1 in terms of cation exchange reactions under varying assumptions of the surrounding rock (exhibiting homogenous and heterogenous transport properties). By this means, the potential impact of the heterogeneity of the rock (water-conductive fractures and local water ingress in the deposition hole) on the water ingress into the buffer could be indirectly assessed. That is, regions of the buffer which have undergone significant variations in their cation exchange composition during the experiment indicate regions of permeable rock or presence of fractures next to them, which will constitute the main groundwater sources for the water saturation of the buffer. The scoping calculations can give insights into the extent of these interaction processes that could be useful to plan the post-mortem characterization campaign upon dismantling.

2 Methodology

The general methodology to be followed in this project stems from the work performed for the Alternative Buffer Material insitu test (ABM), also at Äspö URL (Idiart et al. 2012, 2014, Wallis et al. 2016). In that work, the ABM1 package was analysed and simulated encompassing the thermal evolution of the system, temperature-dependent diffusive transport, and cation exchange reactions resulting from the groundwater-bentonite interaction.

In this scoping study, the model is based on the above-mentioned approach. It has been assumed that the bentonite buffer is fully water saturated with a porewater composition resulting from the mix between the original bentonite porewater and the groundwater (at the given temperature) with fractions calculated from the initial degree of saturation. In this model, mineral reactions for anhydrite and calcite) were considered in addition to cation exchange reactions, and sensitivity cases were run to study the effect of the surrounding rock and fractures. Diffusion in the buffer is temperature dependent. A constant temperature field was calculated as a first step to be used in the reactive transport simulations.

2.1 Conceptual model

The dry density of the buffer at installation was 1570 kg/m^3, but this value increases during the experiments reaching an average value of 1650 kg/m^3 (measured after dismantling cells 5 and 6, Olsson et al. 2013). The development of the dry density seems to take place in a short period of time (a few years), so we have used the final value in the reactive transport models. This value of dry density results in a porosity of 0.406 (considering a grain density of 2780 kg/m^3). The buffer properties are summarized in Table 2-1.

Table 2-1. Properties of the buffer considered for the reactive transport models of deposition hole 1 of the Prototype Repository.

Property	Value
Grain density (kg/m^3)	2780
Dry density (kg/m^3)	1650
Porosity	0.406
Initial water content (% weight)	17 %
Initial saturation	0.70
Effective diffusion coefficient (m^2/s)*	$1.12 \cdot 10^{-10}$ – $3.60 \cdot 10^{-10}$

**Range of temperatures expected in the buffer (30-75 ºC)*

A simplified geochemical system composed of basic cations (Na^+, Ca^{+2}, Mg^{+2} and K^+) and three anions (HCO_3^-, SO_4, Cl^-) is assumed. In addition, calcite and anhydrite are considered as accessory minerals. The effective diffusion coefficient is estimated as a function of the dry density as proposed by Ochs and Talerico (2004):

$$D_e(\rho_d) = 6.7785 \cdot 10^{-9} \cdot \exp(-0.0025671 \cdot \rho_d) \quad (2.1)$$

where ρ_d is the dry density of the bentonite. The effect of temperature on effective diffusivity is estimated using the empirical formula proposed by Wersin et al. (2014):

$$D_e(T) = D_e(T_0) \cdot exp(0.026 \cdot T) \quad (2.2)$$

Aqueous speciation and mineral reactions are calculated with the Thermochimie version 11 thermodynamical database (Giffaut et al. 2014). Cation exchange reactions, on the other hand, are accounted for in the buffer using the selectivity coefficient values that are summarized in Table 2-2 (Bradbury and Baeyens 2002).

Table 2-2. Cation exchange selectivity coefficients proposed for MX80 bentonite by Bradbury and Baeyens (2002).

Selectivity Coefficient	Value
K_{NaK}	4.0
K_{NaCa}	2.6
K_{NaMg}	2.2

The initial amount of the mineral phases considered are 0.70 mass% gypsum (modelled as 0.55 mass% anhydrite) and 0 mass% calcite, according to data provided by SKB. Anhydrite is chosen as the sulphate phase due to the relatively high temperatures reached in the buffer. In the colder areas of the buffer gypsum is expected to be formed instead, but the effect on cation exchange is considered to be small. The initial cation exchange composition, reported by Olsson et al. (2013) is presented in Table 2-3.

Table 2-3. CEC, initial exchanger composition (Olsson et al. 2013) and composition after saturation with rock groundwaters.

	Initial (%)	Initial (meq/100g)	Saturated (%)	Saturated (meq/100g)
CEC (meq/100g)		85		85
Ca	20.0	17.00	21.1	17.91
Na	69.0	58.65	68.1	57.85
Mg	9.0	7.64	8.9	7.55
K	2.0	1.70	2.0	1.69

At the start of the experiments, the bentonite buffer has a saturation of 0.61 (17 % water content and dry density of 1570 kg/m^3, according to Dohrmann and Kaufhold 2014) and is hydrated naturally by the surrounding granitic groundwater. Monitoring of the pressure and relative humidity of the buffer shows that this process is relatively fast and takes a few years (Dohrmann and Kaufhold 2014). The saturation of the buffer may have an effect on the exchanger composition of the buffer but, due to the suction of the buffer, this process is expected to be rather fast and homogeneous compared to the diffusive regime and have a relatively small effect on the exchanger composition. Therefore, for this modelling work we have accounted for this process with batch geochemical modelling of the buffer prior to fully saturated reactive transport modelling, detailed below.

The initial porewater composition of the bentonite buffer has been calculated from the mix between the original bentonite porewater and the groundwater, considering mix fractions calculated from the initial degree of saturation. This porewater has been equilibrated with the mineral phases considered in the model as well as with the cation exchange composition of the interlayer (see Table 2-3). The resulting porewater, as well as the buffer porewater at installation and the Äspö groundwater compositions are summarized in Table 2-4. The cation exchange composition is affected by this process, but in less than 1 %, see Table 2-3.

Table 2-4. Buffer porewater at installation and Äspö groundwater as in Karnland et al. (2009), and calculated buffer porewater composition after it reaches full saturation.

	Buffer porewater at installation (Karnland et al. 2009)	Äspö groundwater (Karnland et al. 2009)	Buffer porewater – Saturated
Temperature (ºC)	15	15	60
pH	7.86	6.9	7.23
Ca (mol/kgw)	1.01E-02	5.60E-02	1.07E-02
Cl (mol/kgw)	5.12E-02	1.99E-01	9.65E-02
C (mol/kgw)	1.05E-03	4.40E-04	8.56E-04
Na (mol/kgw)	2.12E-01	9.60E-02	1.66E-01
Mg (mol/kgw)	5.81E-03	1.60E-03	5.57E-03
K (mol/kgw)	1.40E-03	2.60E-04	1.20E-03
S(6) (mol/kgw)	9.65E-02	6.00E-03	5.11E-02

Regarding the host rock, this material has been modelled with 0.3 % porosity (Rhén and Forsmark 2001, reported values between 0.2 and 0.4 %) and an effective diffusion coefficient of 10^{-13} m^2/s (Ohlsson and Neretnieks, 1997). The models only consider chemical interactions between the buffer and the rock, the canister and backfill boundary conditions are assumed closed to solute transport.

2.2 Modelling cases and implementation

2.2.1 General specifications

The thermo-hydro-chemical (THC) models are implemented in PFLOTRAN (Hammond et al. 2014), an open-source, state-of-the-art massively parallel subsurface flow and reactive transport code. It solves a system of generally nonlinear partial differential equations describing multiphase, multicomponent and multiscale reactive flow and transport in porous materials. In future work, this could enable us to extend the modelling to THC processes at larger scale and considering the hydro-thermal transient phase. The massively parallel coding would also allow the simulation of the whole Prototype Repository. As shown previously in Figure 1-1, the Prototype Repository consists of 6 boreholes, divided into 2 sections, sealed with concrete plugs. Each borehole contains a full-size bentonite buffer and a canister with a heat source to simulate the heat produced by nuclear waste. The diameter of a deposition hole is 1.75 m and its length is ~7 m. The inner diameter of the ring-shaped blocks is ~1.07 m. Each buffer consists of 35 cm thick rings of compacted bentonite (MX-80). Considering these specifications, a 3D geometry (Figure 2-1) that includes the buffer and, in some modelling cases, 10 m of the surrounding rock and a fracture, are built in GiD (Coll et al. 2018) for one borehole (borehole 1).

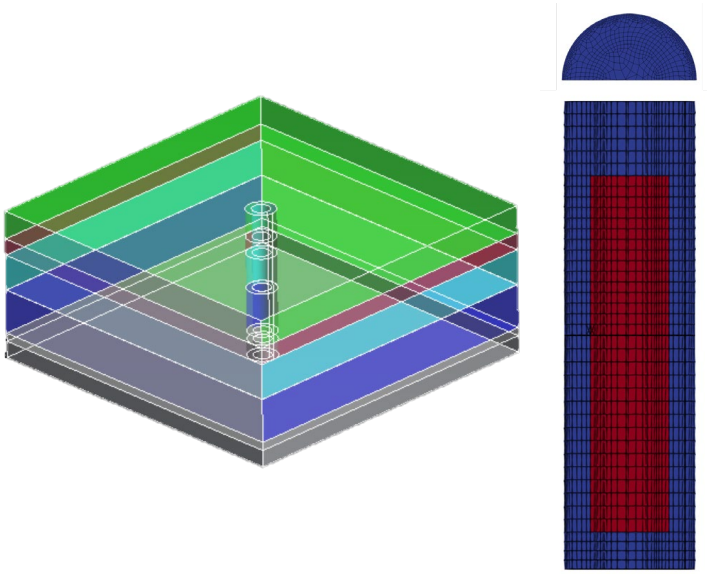

Figure 2-1. *Domain around the borehole (left panel) and mesh in the bentonite buffer and canister (right panel).*

Prior to the reactive transport modelling, the steady-state temperature field of the buffer was obtained using a heat transfer model. The heat transfer parameters of the rock and buffer are outlined in Table 2-5.

Table 2-5. Heat transfer model parameters. The porosity values are as for the reactive transport models, the thermal conductivities and heat capacities as the modelling work carried out in Malmberg and Åkeson (2022).

Parameter	Buffer	Rock
Porosity (-)	0.406	0.003
Thermal conductivity (W/m·K)	1.3	2.685
Heat capacity (J/kg·K)	800	770

The heat transfer model considered a fixed temperature of 15 ºC at the lateral external surfaces of the rock, thermal insulation at the top and bottom boundaries of the rock and a fixed temperature of 75 ºC at the canister – buffer interface. The resulting temperature field, shown in Figure 2-2, has been compared to the monitored data in borehole 1 (Goudarzi 2022). The modelled temperature is somewhat higher directly above and below the canister, but otherwise the results match the experimental observations. Overall, the obtained temperature field seems to be an acceptable approximation of the experimental conditions for the purpose of this study. This temperature field is used in the different modelling cases described in the following sections.

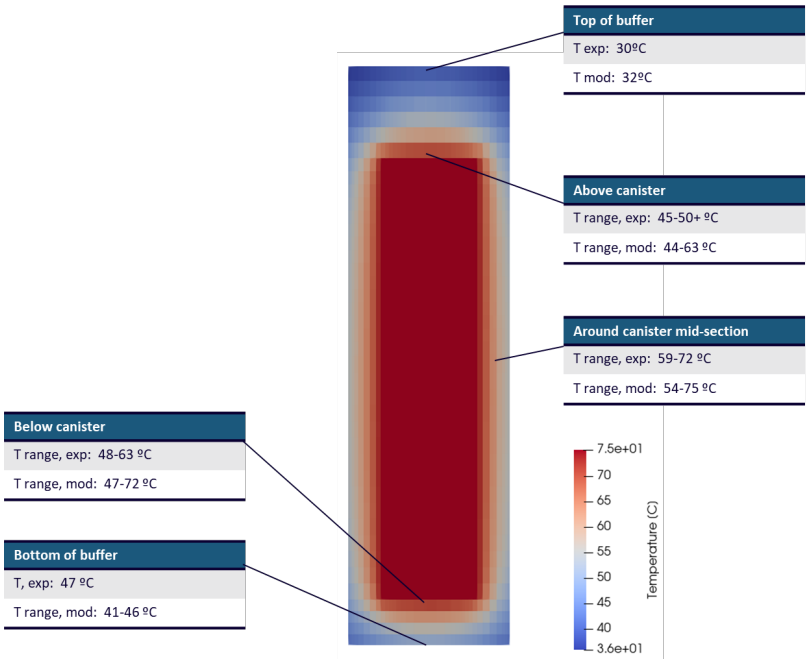

Figure 2-2. *Steady-state temperature field obtained with the heat transfer model. Comparison between model results and monitored data (Goudarzi 2022).*

2.2.2 Baseline model

The baseline case considers only the buffer (the canister is included in the geometry but is chemically inert and closed), with a Dirichlet boundary condition at the buffer-rock interface that corresponds to the groundwater composition. This case represents a scenario of fast groundwater renewal around the deposition hole and constitutes a bounding case with high amounts of cation exchange.

A semi-structured mesh has been generated, which is displayed in Figure 2-3. The mesh of the buffer and canister consists of 70 000 elements and is refined at the buffer-rock interface with element sizes of 2 cm.

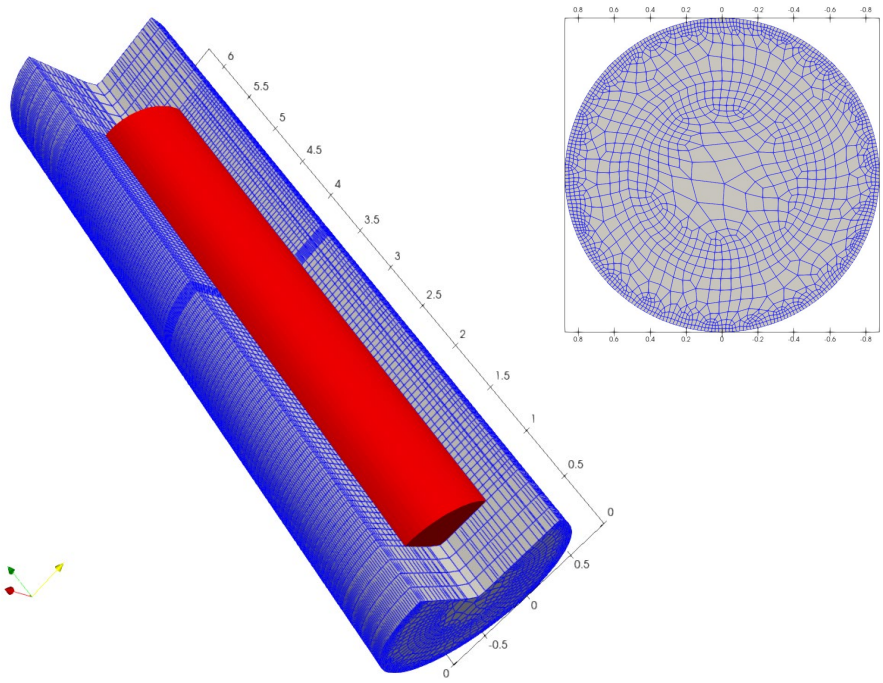

Figure 2-3. *Mesh of the baseline model, generated with GiD (Coll et al. 2018).*

2.2.3 Sensitivity Cases

In the baseline model the buffer-rock interaction is maximized with a Dirichlet boundary condition at the interface. This means that geochemical interactions are not limited by the transport properties of the rock, while in reality this is expected to be the case. A set of sensitivity cases is considered to evaluate the effect of the rock transport properties and their heterogeneity on the cation exchange evolution in the buffer.

Heterogeneous cases

These sensitivity cases include water-bearing features on the periphery of the buffer, modelled by using Dirichlet boundary conditions with the groundwater composition prescribed. The rest of the buffer-rock interface is closed to solute transport. The geometry and mesh used in this case are the same as in the baseline, illustrated in Figure 2-3. Two cases are modelled with different contact areasizes (20 and 5 cm^2) between the buffer and the water-bearing feature (Figure 2-4), in order to test the sensitivity towards this parameter.

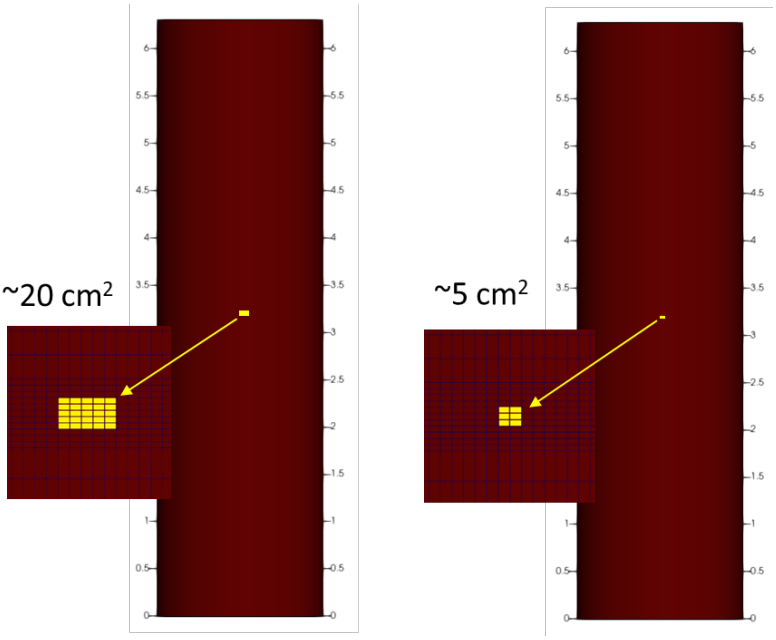

Figure 2-4. *3D geometry used for the heterogeneous sensitivity cases and details of the meshes at the contact areas between the buffer and the water-bearing features.*

Fracture cases

In these sensitivity cases, the host rock includes a horizontal fracture at mid-height of the buffer. With this setup, for most of the buffer-rock contact area the geochemical interaction is limited by the diffusive properties of the rock, whereas there is a small region of the buffer where this interaction is enhanced by the diffusive and advective fluxes taking place in the fracture that crosses it. The modelling setup and properties of each material are presented schematically in Figure 2-5. The generated 3D geometry, shown in Figure 2-6 and Figure 2-7, includes the buffer, backfill and canister, centred in a square section of rock of 20-meter length and a horizontal fracture that crosses the deposition hole. The canister and backfill are included in the model but are chemically inert domains that do not interact with the buffer. The fracture has an aperture of 1 cm, discretized with 3 mesh elements in the vertical direction, which is equivalent to a fracture-buffer interface surface area of 550 cm^2. This aperture size is chosen to keep reasonable element sizes and is quite large compared to typical fracture apertures at the Äspö site. As such, the present sensitivity cases most likely overestimate the interaction between the buffer and rock fractures. An unknown parameter in the present modelling cases is the advective flow through the fracture. In a first step, a set of conservative tracer transport models was carried out with different fracture flow values. Two flow values are selected to carry out full reactive transport simulations: 10^{-6} and 10^{-8} m/s, as outlined in Section 3.2.2.

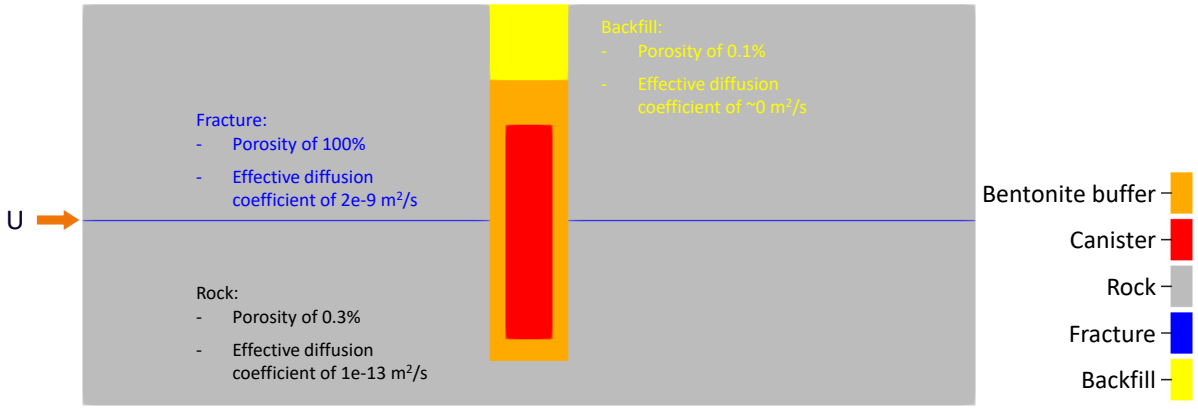

Figure 2-5. *Scheme of the model set up for the fracture sensitivity cases.*

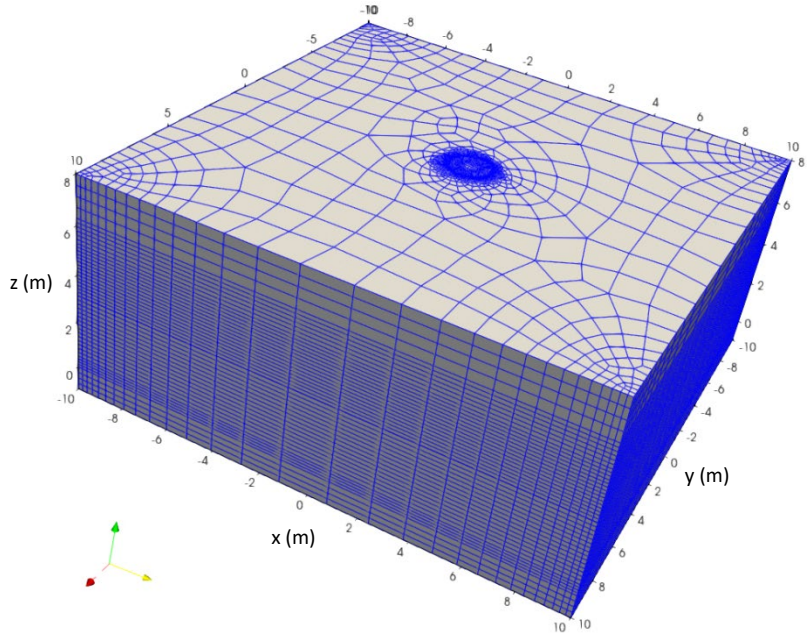

Figure 2-6. *Full 3D geometry and mesh used in the fracture sensitivity cases.*

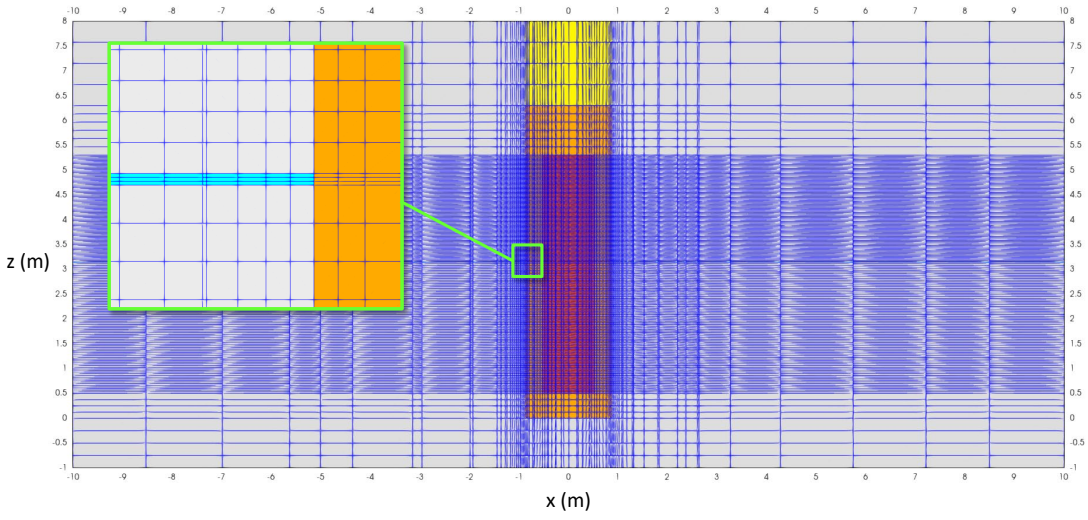

Figure 2-7. *Section of the 3D geometry and mesh used in the fracture sensitivity cases, with a detail of the buffer-fracture interface.*

Rock-limited diffusion

The sensitivity case uses the same geometry and mesh as the fracture cases (Figure 2-6, Figure 2-7). However, the rock-limited case only considers solute transport by diffusion between the buffer and rock. This case presents more realistic cation exchange values for most of the buffer volume.

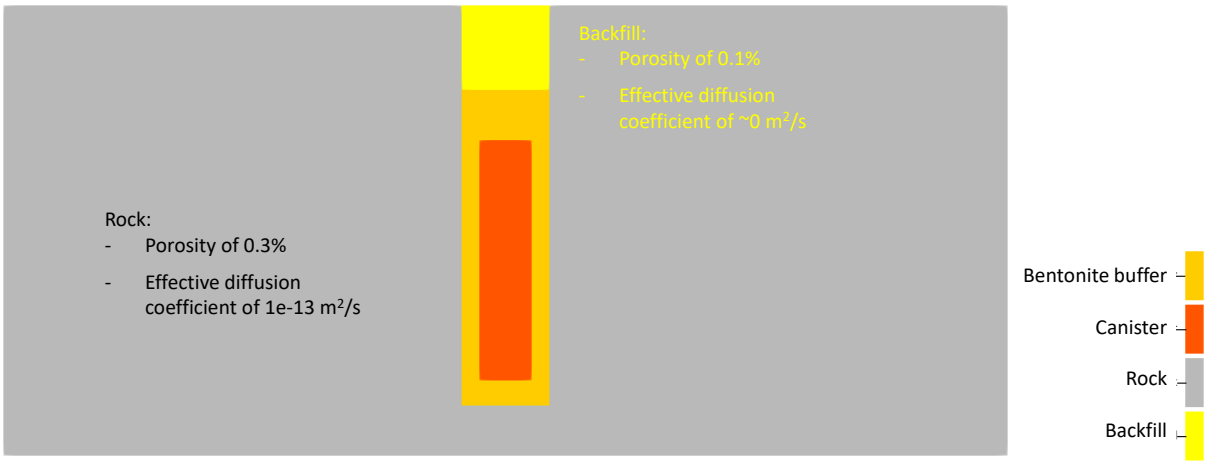

Figure 2-8. *Scheme of the model set up for the rock-limited diffusion case.*

3 Results

The results of the different modelling cases are outlined next in terms of tracer diffusion, mineral concentrations and cation fractions in exchanger in the buffer.

3.1 Baseline model

The results of the baseline simulation are analysed in the following figures. Firstly, the interaction between the rock (groundwater) and the buffer is evaluated with two tracers, Tr1 and Tr2. Tr1 has an initial concentration of 10^{-5} M in the buffer and 10^{-3} M in the groundwater. For the second tracer, Tr2, the initial concentrations are reversed with 10^{-3} M in the buffer and 10^{-5} M in the groundwater. Figure 3-1 and Figure 3-2 show the spatial concentration distribution of the two tracers at different times. After 1 year of simulation, solute transport seems to have affected only the outer part of the buffer that is in contact with the host rock. After 20 years, however, the in-diffusing tracer reaches most of the buffer volume and only the section above the canister presents low concentrations. The opposite is true for the out-diffusing tracer, Tr2.

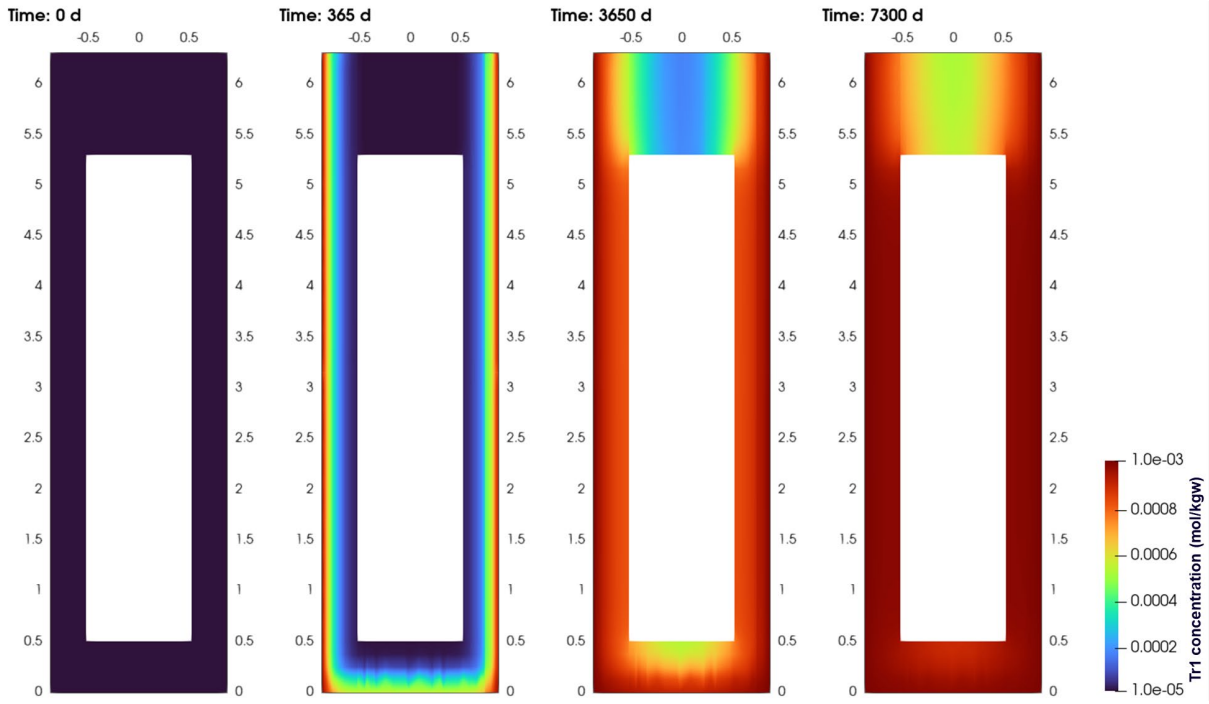

Figure 3-1. *Concentration of tracer Tr1 in the buffer (in mol/kgw) at different times (0, 1, 10 and 20 years) obtained with the baseline model.*

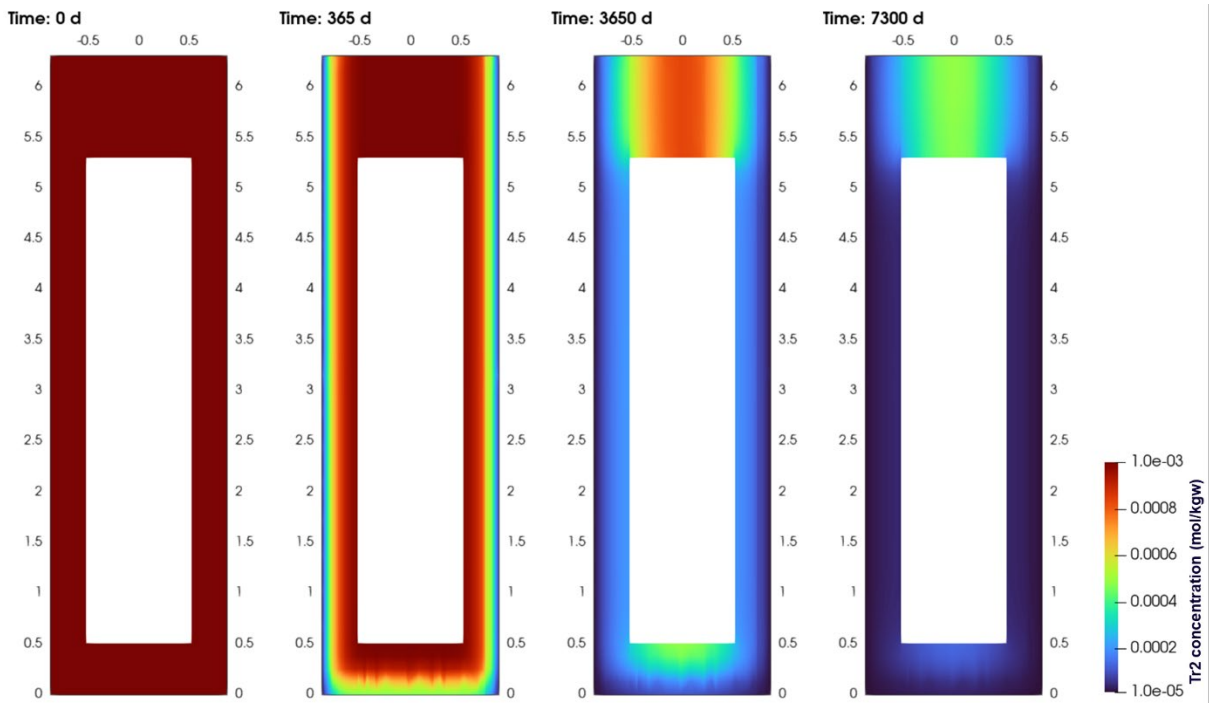

Figure 3-2. *Concentration of tracer Tr2 in the buffer (in mol/kgw) at different times (0, 1, 10 and 20 years) obtained with the baseline model.*

The temporal evolution of tracer concentrations indicates the degree of diffusive mixing that is taking place in the buffer between buffer porewater and groundwater. Figure 3-3 shows the equivalent amount of external solution that is diffusing into the buffer and the buffer porewater that is diffusing out of it. As can be observed, the two curves exhibit opposite trends, as one porewater replaces the other. Initially, the large concentration gradients at the rock-buffer interface result in a relatively fast displacement. In the long term, however, the gradients are less pronounced and the buffer porewater is almost fully replaced by groundwater.

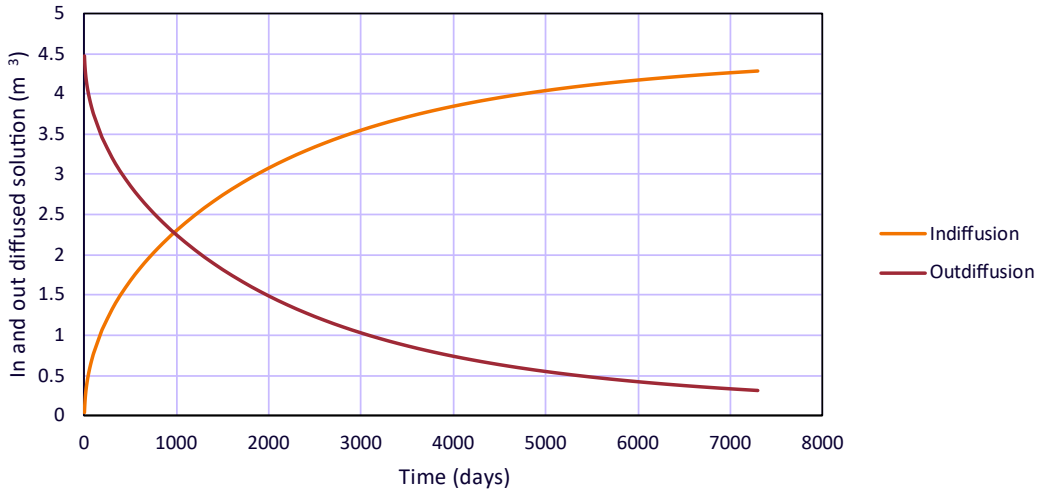

Figure 3-3. *Temporal evolution of the equivalent in-diffused groundwater and out-diffused buffer porewater, in m^3, obtained with the baseline model.*

Regarding the mineral phases in the buffer, the interaction with the groundwater results in anhydrite dissolution near the interface with the rock (Figure 3-4), due to aqueous sulphate outflow (Figure 3-5). Small amounts of anhydrite precipitation are observed next to the canister due to the thermal gradient imposed in the buffer. No precipitation of calcite has been observed during the 20 years of simulation in this modelling case.

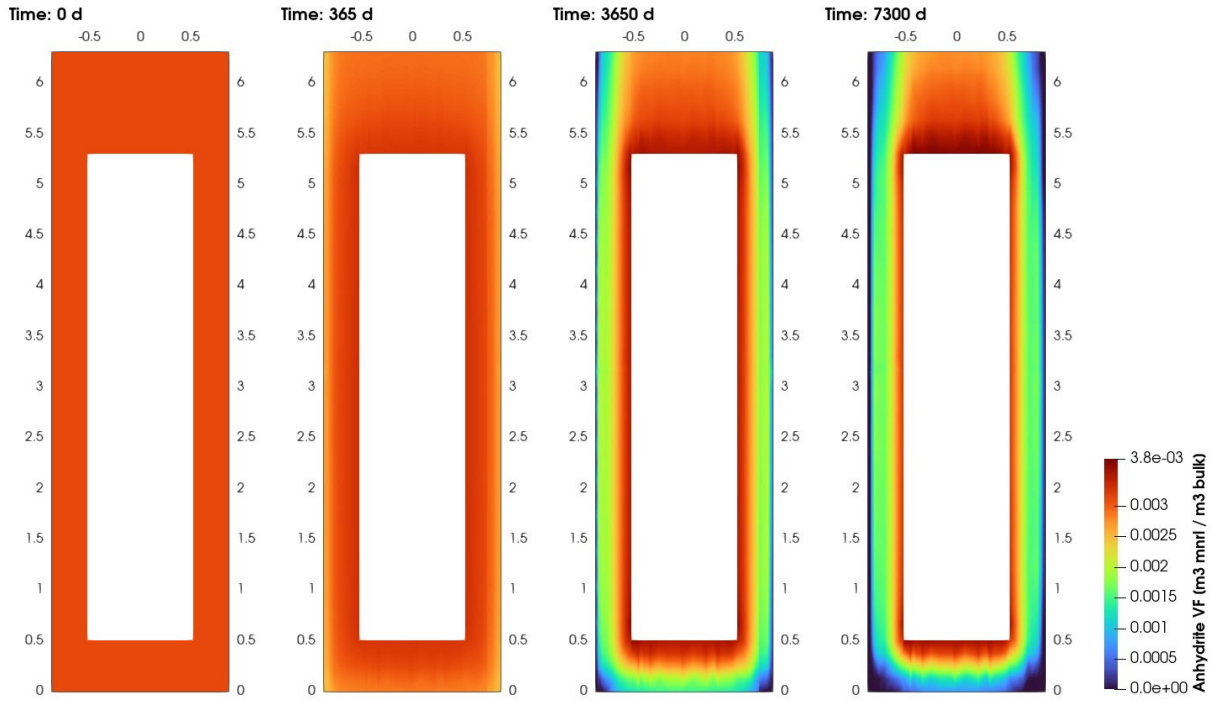

Figure 3-4. *Volume fraction of anhydrite in the buffer at different times (0, 1, 10 and 20 years) for the baseline model.*

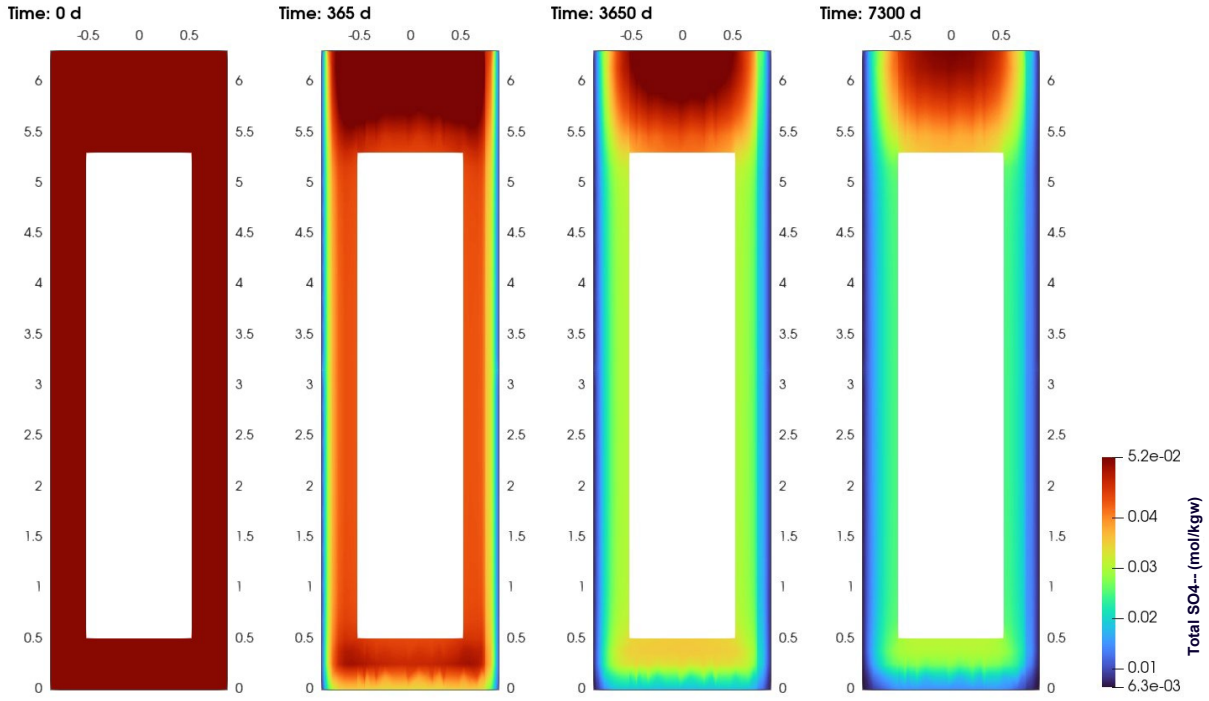

Figure 3-5. *Aqueous concentration of sulphate (in mol/kgw) at different times (0, 1, 10 and 20 years) for the baseline model.*

In terms of cation exchange composition, calcium replaces the other cations in a front that advances from the buffer-rock interface into the buffer. Figure 3-6 shows the evolution of the cation exchange composition at three locations in the buffer. Next to the rock (2 cm from the buffer-rock interface, point A in the figures), calcium becomes the major cation after only 2 years. After 20 years, the exchanger is occupied by 63 % calcium, 33 % sodium and minor fractions of K and Mg. Away from the buffer-rock interface, however, the effect on the exchanger is minor. The cation exchange front seems to start affecting a point directly next to the canister (point B) by the end of the experiment, but to a very small extent. A point at the centre of the buffer and above the canister (point C) seems to be unaffected even at final times. It is worth pointing out that the initial composition of the exchanger is

affected by the temperature distribution in the buffer. At the point next to the canister, the high temperatures affect anhydrite solubility and, as a result, the initial fraction of calcium in exchanger is slightly lower than at other points.

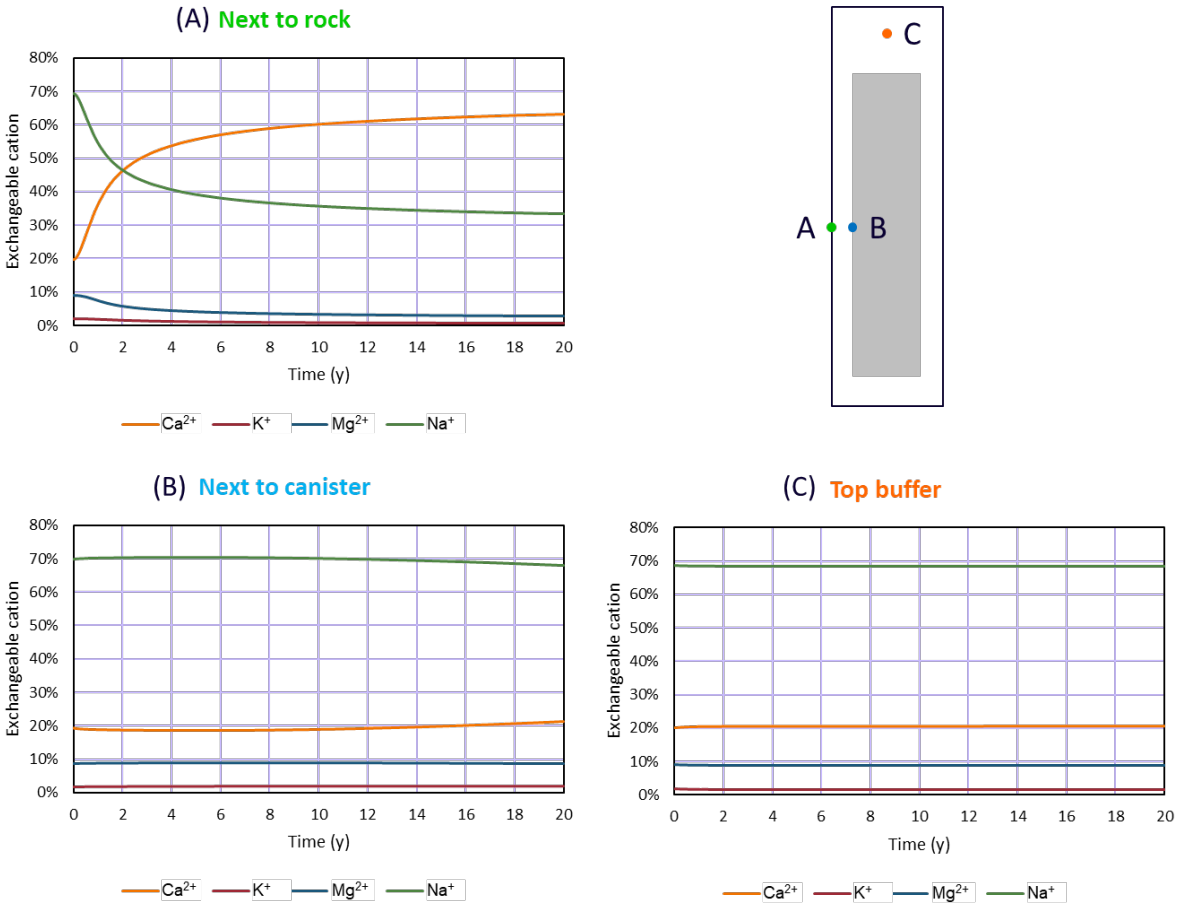

Figure 3-6. *Temporal evolution of the cation exchange composition, in % of each cation, at three locations in the buffer obtained with the baseline model.*

Figure 3-7 to Figure 3-10 show the spatial distribution of each cation in the exchanger at different times (0, 1, 10 and 20 years). After 20 years, the front has advanced about 10 cm. In the rest of the buffer, the composition of the exchanger remains more or less constant.

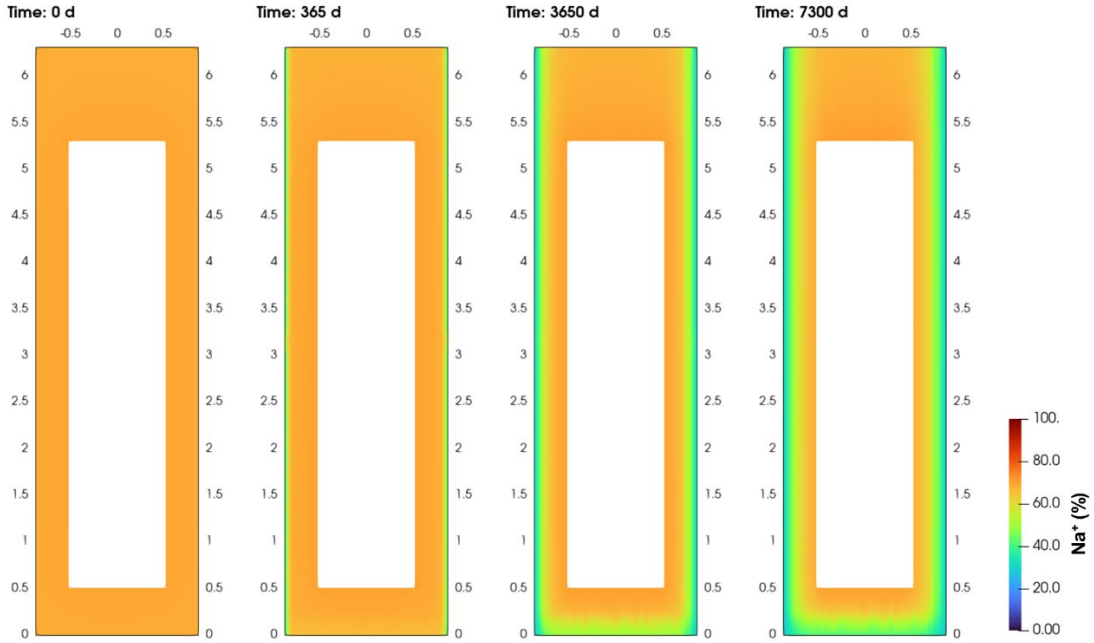

Figure 3-7. *Sodium fraction in exchanger (in %) in the buffer at different times (0, 1, 10 and 20 years) obtained with the baseline model.*

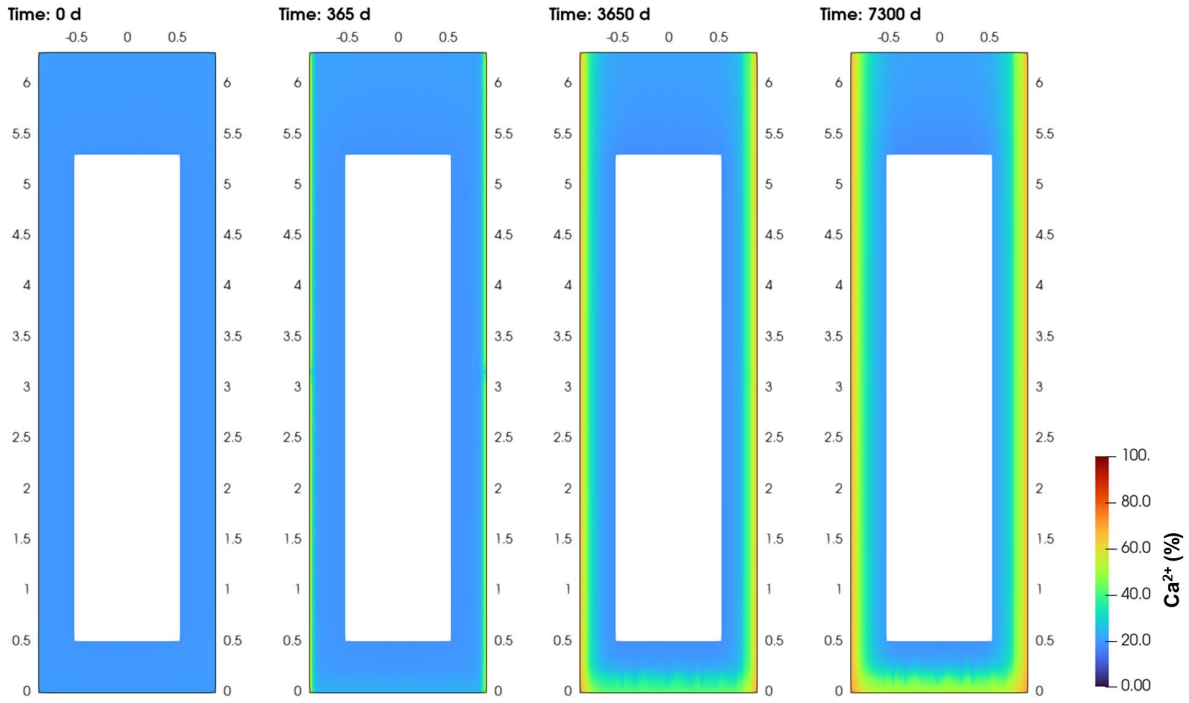

Figure 3-8. *Calcium fraction in exchanger (in %) in the buffer at different times (0, 1, 10 and 20 years) obtained with the baseline model.*

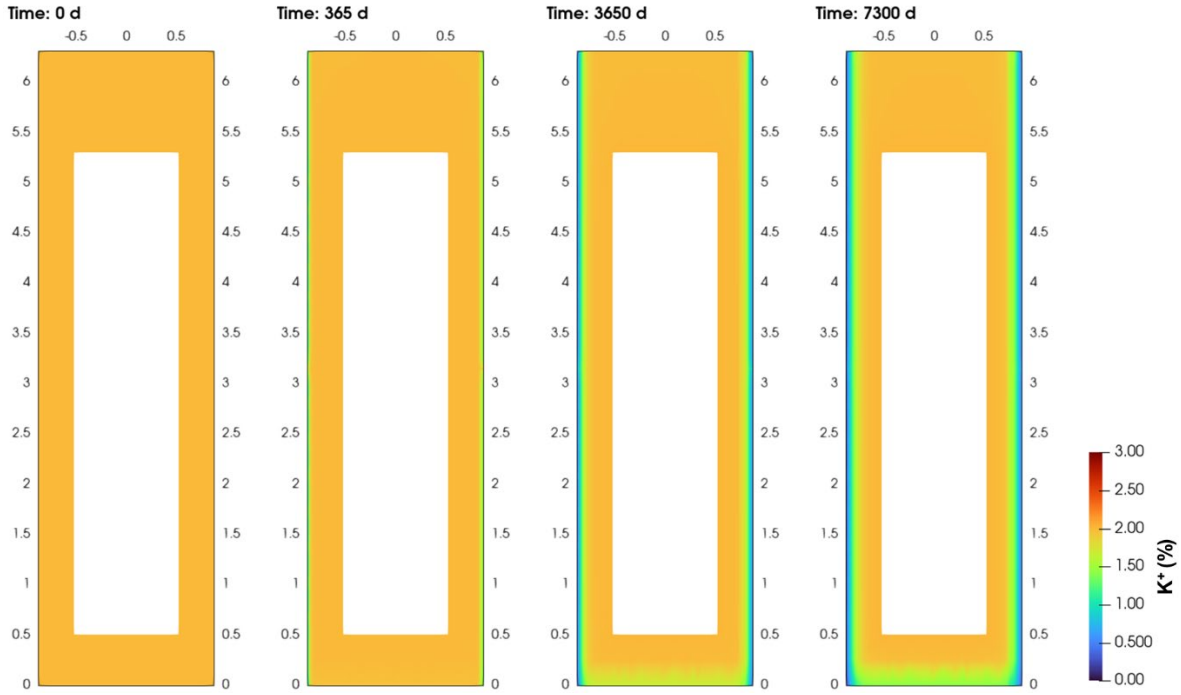

Figure 3-9. *Potassium fraction in exchanger (in %) in the buffer at different times (0, 1, 10 and 20 years) obtained with the baseline model.*

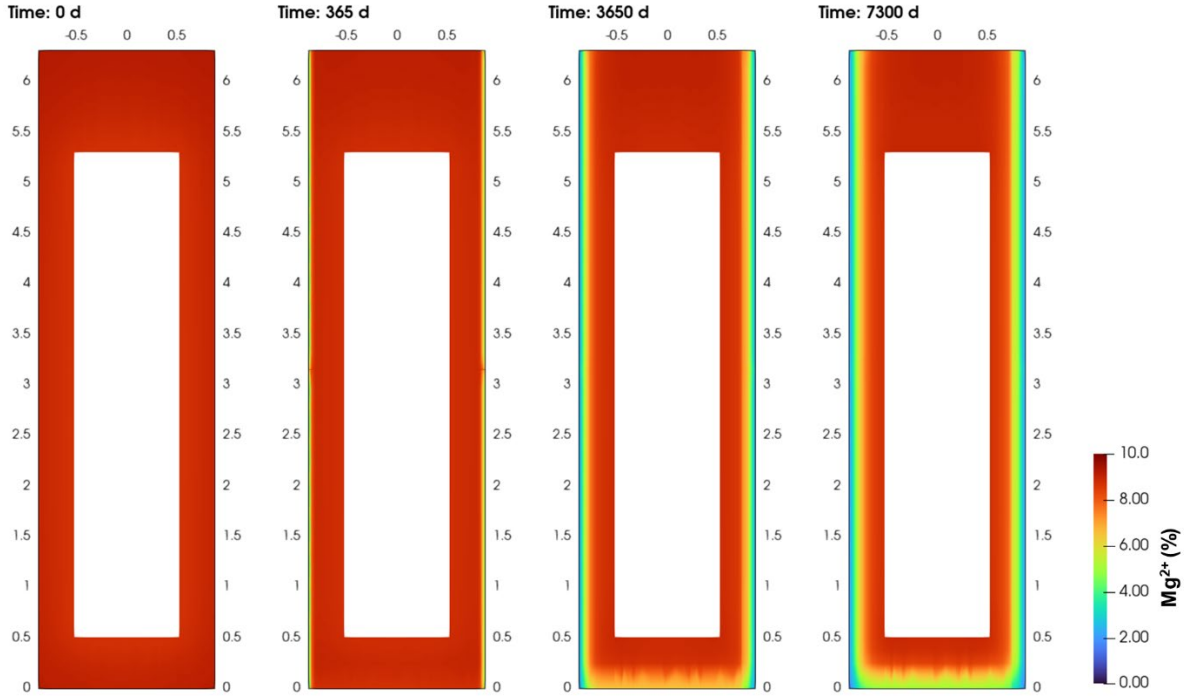

Figure 3-10. *Magnesium fraction in exchanger (in %) in the buffer at different times (0, 1, 10 and 20 years) obtained with the baseline model.*

Finally, the radial distribution of the cation exchange composition is shown in Figure 3-11. After 20 years, calcium has replaced the other cations in the outer 10 cm of the buffer and becomes the major cation (reaching 65 % at the interface with the rock). The sodium, magnesium and potassium fractions decrease at the interface with the rock to values of 32 %, 2.4 % and 0.6 %, respectively. The profiles show smooth cation exchange fronts that extend up to 25 cm from the interface with the rock and that exchange slows down with time (not much difference observed between 10 and 20 years).

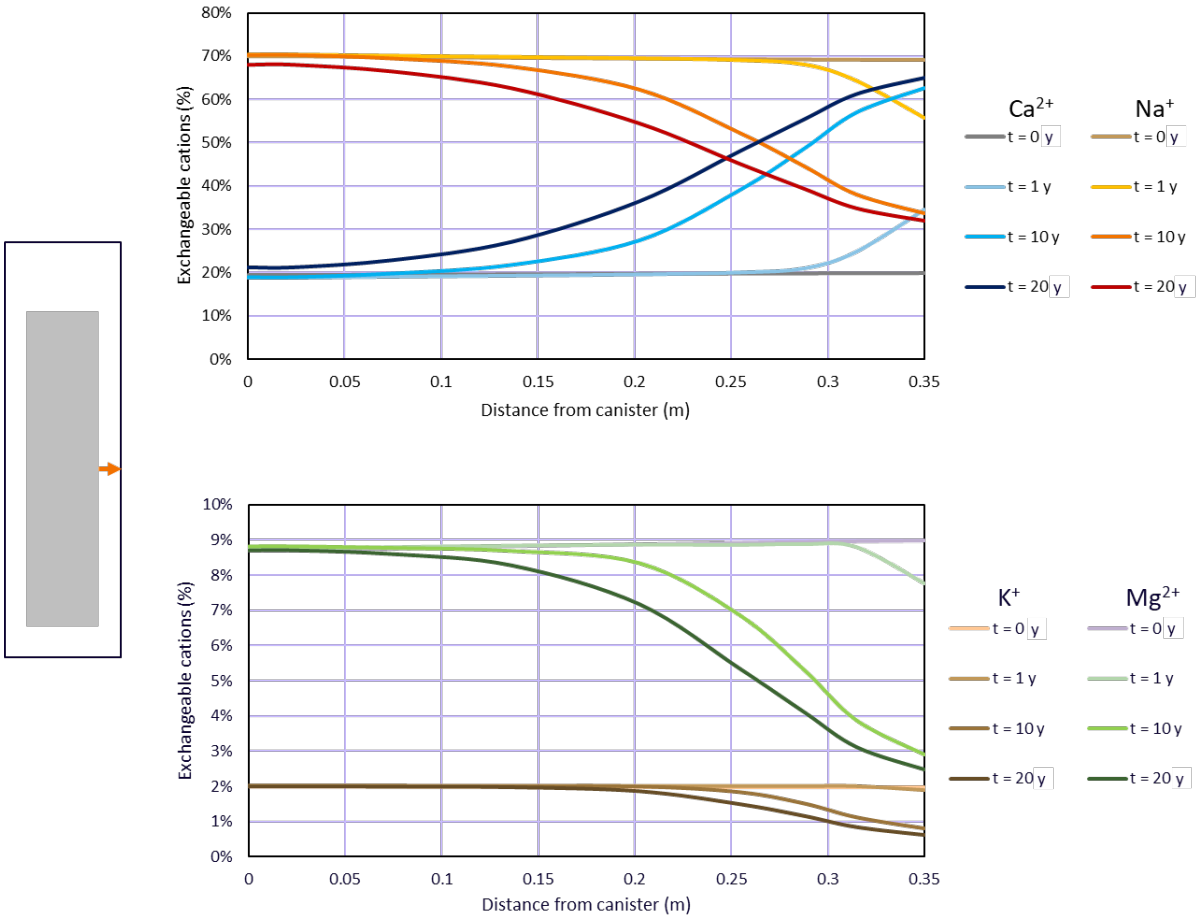

Figure 3-11. *Radial profiles, at the mid-height of the buffer, of the exchangeable cation composition (in %) obtained with the baseline model at different times (0, 1, 10 and 20 years).*

3.2 Sensitivity Cases

3.2.1 Heterogeneous cases

The heterogeneous sensitivity cases consider buffer-rock interaction only over a small area of the buffer-rock interface. Two cases were tested, with contact areas of 20 and 5 cm^2. First, the results of Tr1 concentration evolution are shown in Figure 3-12 and Figure 3-13, for each of the cases. Recall that Tr1 is a tracer that diffuses from the rock into the buffer. Very small amounts of tracer are observed, even after 20 years, especially when compared to the baseline case (see Figure 3-1). Tr1 concentration increases are limited to the first 10 cm closest to the contact area with the groundwater. Comparing Figure 3-12 and Figure 3-13 it is evident that the contact area size does have an impact on the tracer diffusion into the buffer. The evolution of the out-diffusing tracer (Tr2) has not been analysed here as the baseline case showed that its behaviour was inverse to that of Tr1.

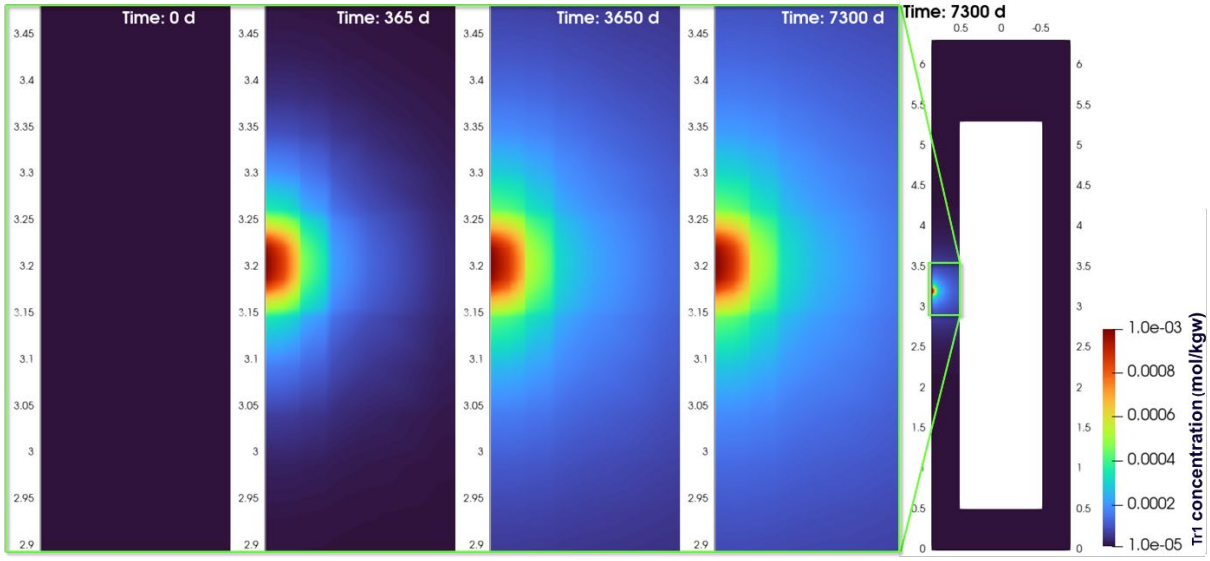

Figure 3-12. *Concentration of tracer Tr1 in the buffer (in mol/kgw) at different times (0, 1, 10 and 20 years) obtained for the heterogeneous case in which the contact area is equal to 20 cm^2.*

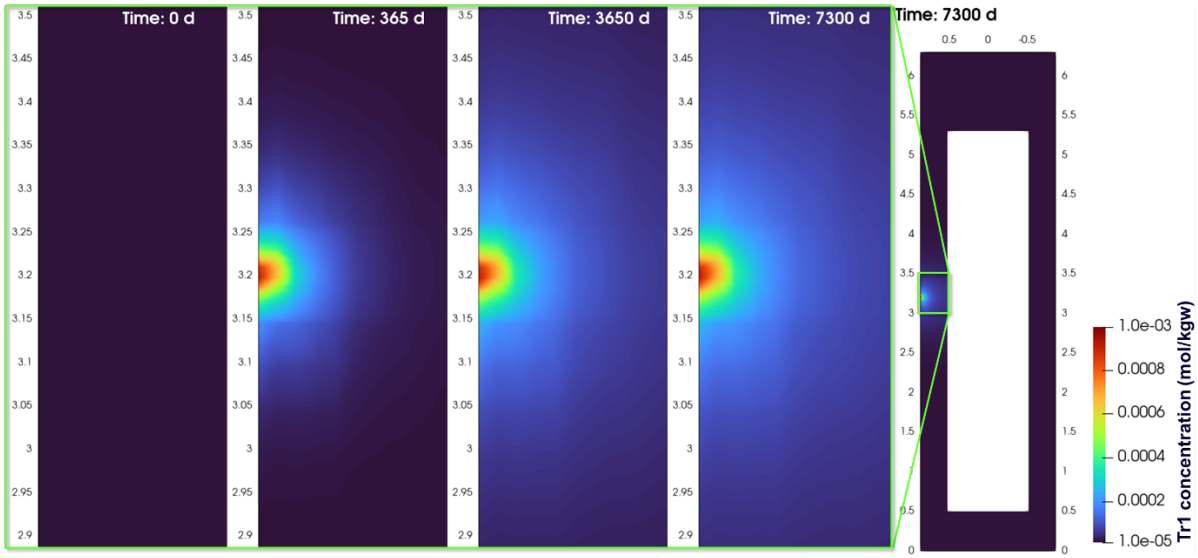

Figure 3-13. *Concentration of tracer Tr1 in the buffer (in mol/kgw) at different times (0, 1, 10 and 20 years) obtained for the heterogeneous case in which the contact area is equal to 5 cm^2.*

Figure 3-14 shows the equivalent in-diffused external solution into the buffer, as calculated from the Tr1 concentrations. In the heterogeneous cases, the mixing between porewaters is very limited and follows a linear tendency with time as the original buffer porewater is far from being replaced (low amounts of Tr1 in the buffer). It is also worth pointing out that the effect is not proportional to the contact area size: a factor 4 increase in contact area size (5 vs 20 cm2) resulted in roughly 2.2 times the amount of in-diffused solution (0.006 vs 0.013 m3).

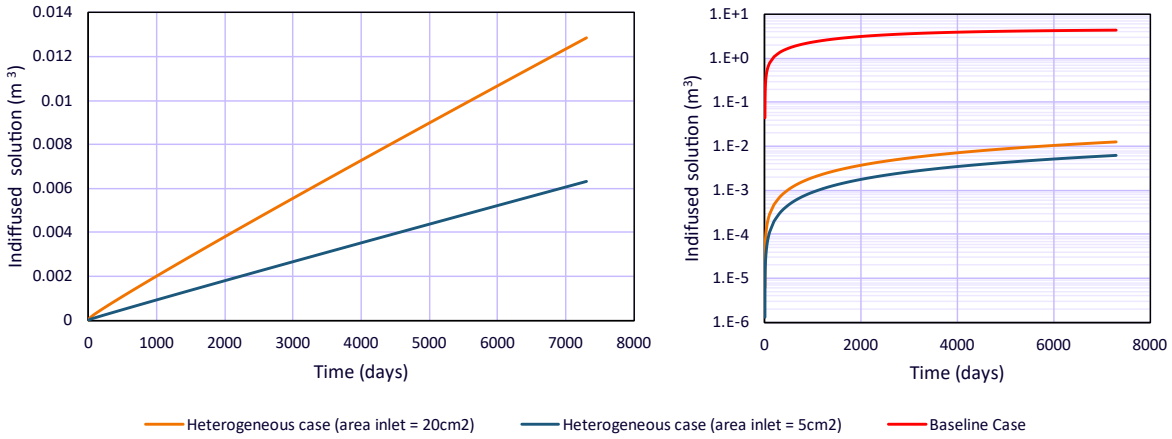

Figure 3-14. *Temporal evolution of the equivalent in-diffused groundwater into to the buffer, in m^3, obtained for the heterogeneous cases. The graph on the right compares the results to those obtained with the baseline model.*

The evolution of anhydrite volume fraction in the buffer obtained for the two heterogeneous cases is displayed in Figure 3-15 and Figure 3-16. It can be observed that anhydrite precipitates slightly next to the heater and in larger quantities around the contact area. This behaviour is in contrast with the baseline results, where anhydrite dissolved next to the buffer-rock interface (Figure 3-4). This behaviour can be explained by considering the evolution of aqueous SO_4^{2-} in the buffer. Figure 3-17 and Figure 3-18 show the spatial distribution of aqueous SO_4^{2-} obtained for the two heterogeneous cases. In the baseline modelling case, the sulphate diffuses out from the buffer over the whole buffer-rock interface (Figure 3-5). In the heterogeneous cases, on the other hand, the sulphate only diffuses out at the contact area and in-diffusing calcium encounters high sulphate concentrations, which results in anhydrite precipitation.

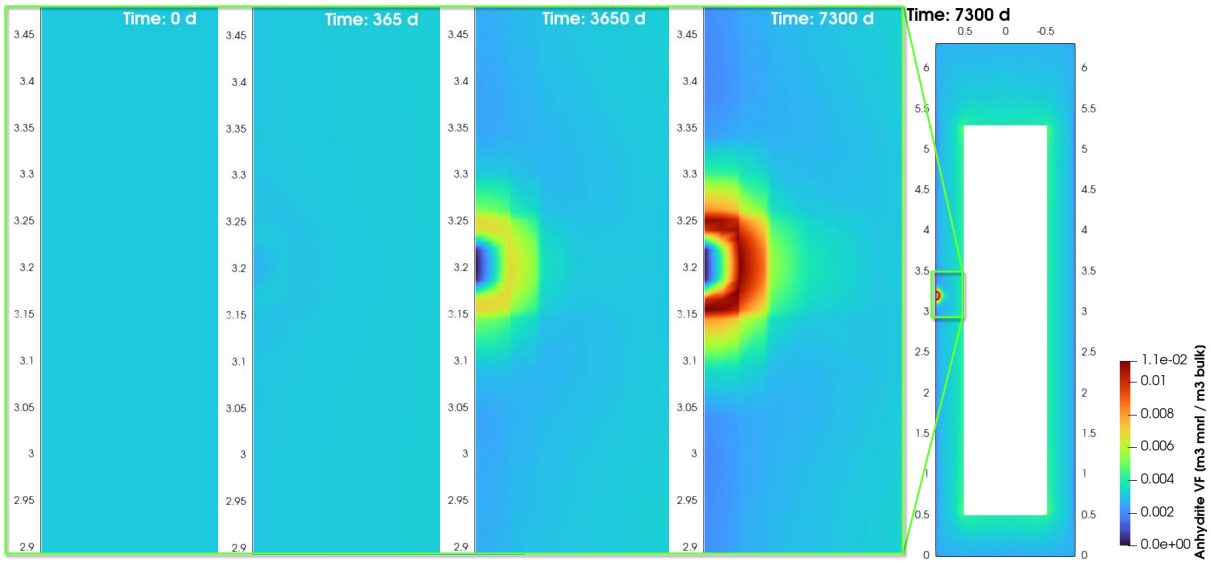

Figure 3-15. *Volume fraction of anhydrite in the buffer at different times (0, 1, 10 and 20 years) obtained for the heterogeneous case in which the contact area is equal to 20 cm^2.*

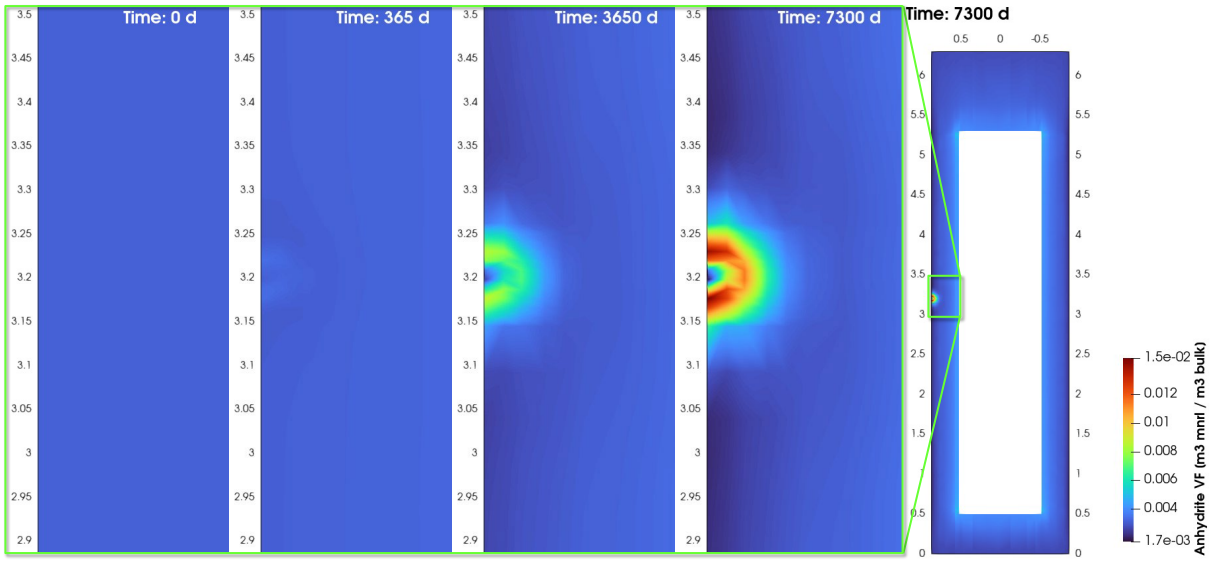

Figure 3-16. *Volume fraction of anhydrite in the buffer at different times (0, 1, 10 and 20 years) obtained for the heterogeneous case in which the contact area is equal to 5 cm^2.*

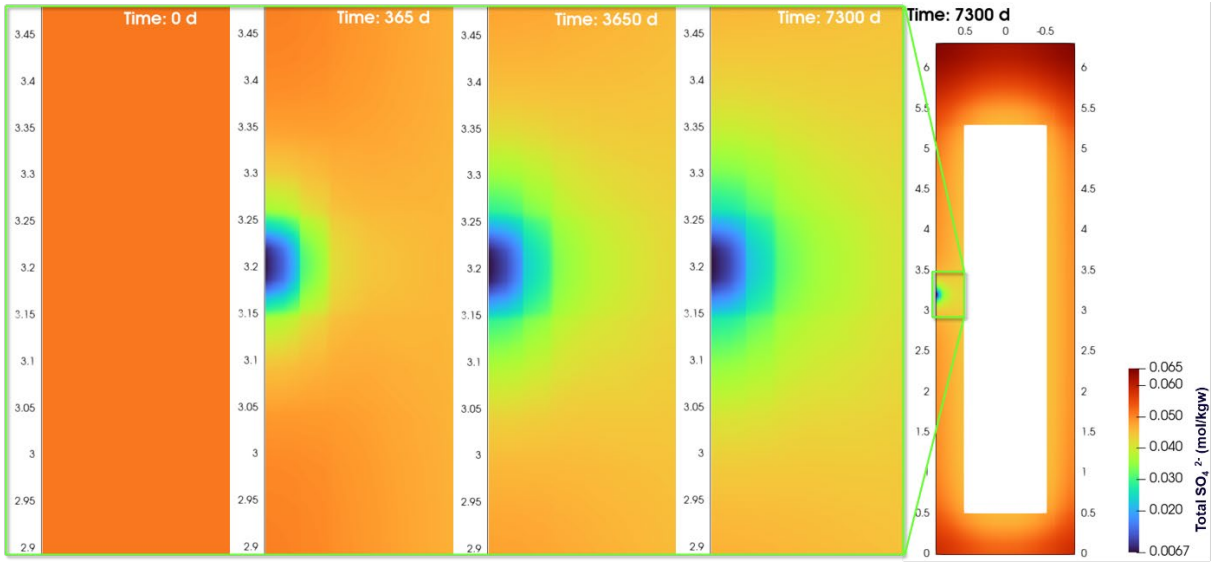

Figure 3-17. *Aqueous concentration of sulphate (in mol/kgw) at different times (0, 1, 10 and 20 years) obtained for the heterogeneous case in which the contact area is equal to 20 cm^2.*

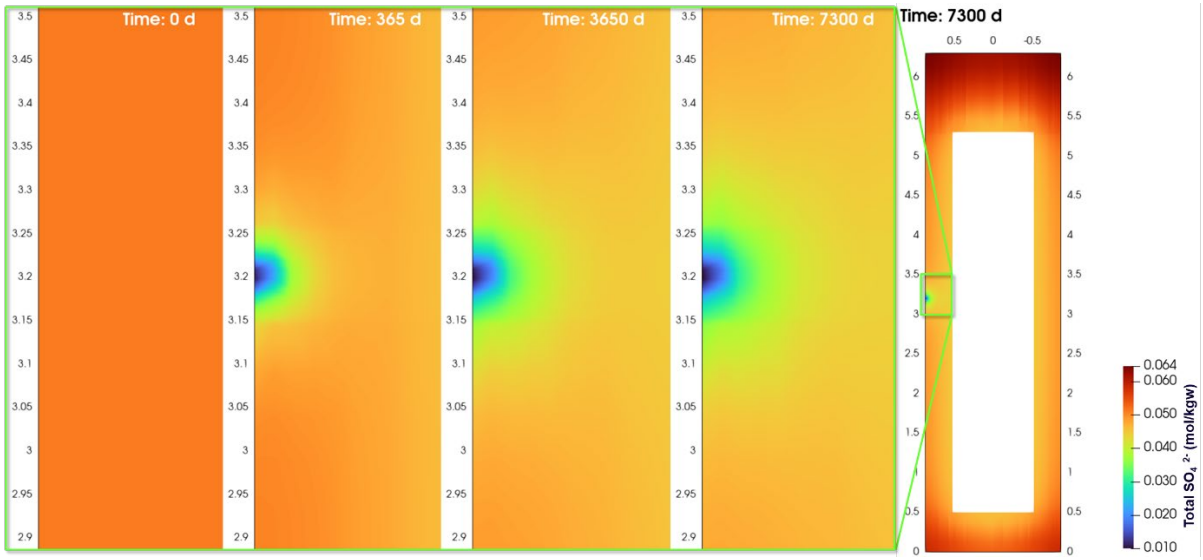

Figure 3-18. *Aqueous concentration of sulphate (in mol/kgw) at different times (0, 1, 10 and 20 years) obtained for the heterogeneous case in which the contact area is equal to 5 cm^2.*

The cation exchange composition next to the buffer-rock contact area (point A in Figure 3-6) is shown in Figure 3-19. Initially, there is a relatively fast Ca-Na exchange (first 2 years) that slows down with time. Calcium replaces the other cations until becoming the major cation in the case with the contact area equal to 20 cm^2, while sodium remains the major cation during the whole experiment for the case with the contact area equal to 5 cm^2. Figure 3-20, Figure 3-21, Figure 3-22 and Figure 3-23 show the spatial distribution of each exchangeable cation at final time (20 years) and the detail vicinity of the contact area at different times (0, 1, 10 and 20 years) for the case with a size of 20 cm^2. Figure 3-24, Figure 3-25, Figure 3-26 and Figure 3-27 show the results for the case with the area equal to 5 cm^2. As illustrated in these figures, away from this contact area changes in the exchanger are negligible in the buffer. Cation exchange is lower in the case with a smaller contact area, as expected.

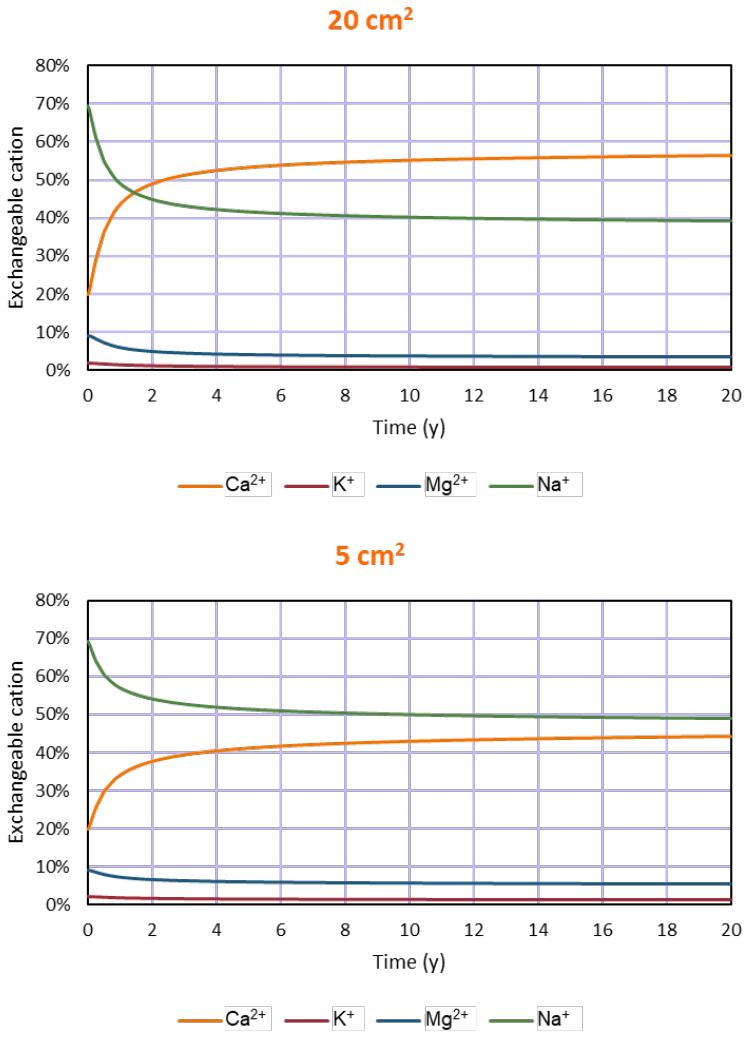

Figure 3-19. *Temporal evolution of the cation exchange composition (in %) 2 cm from the buffer-rock interface (point A in Figure 3-6) obtained for the heterogeneous cases that consider a contact area of 20 cm² (top) and 5 cm² (bottom).*

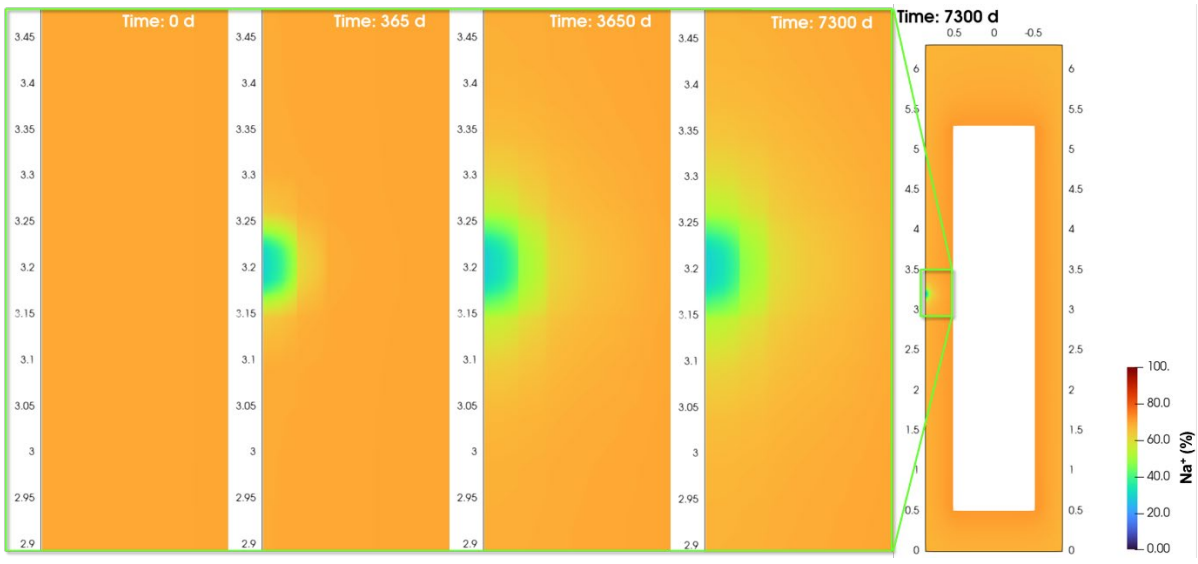

Figure 3-20. *Sodium fraction in exchanger (in %) in the buffer at different times (0, 1, 10 and 20 years) obtained for the heterogeneous case in which the contact area is equal to 20 cm².*

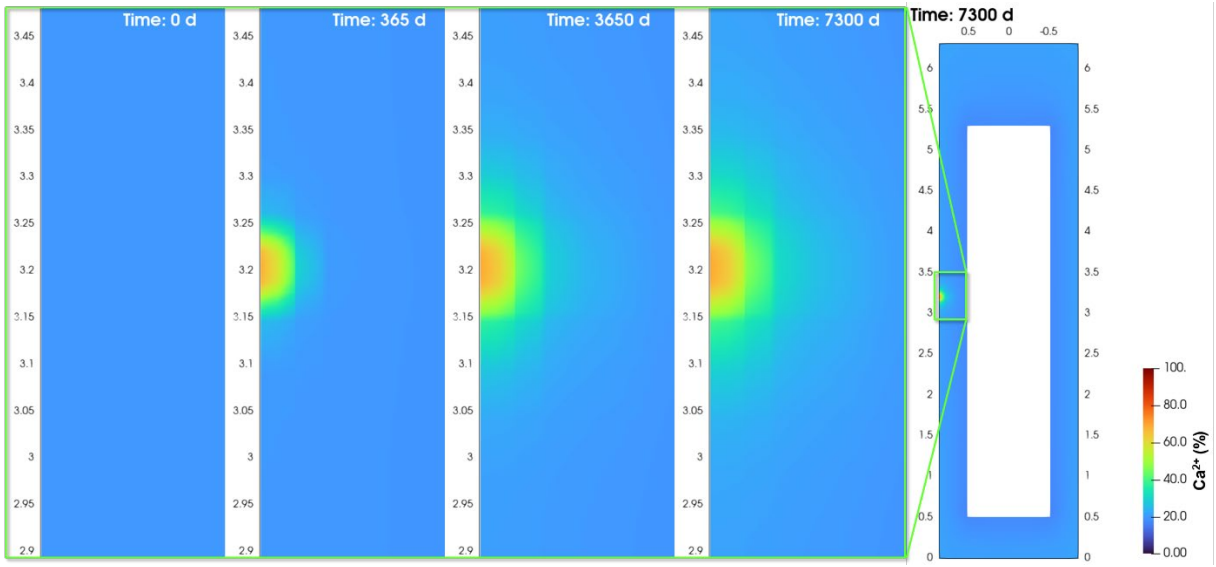

Figure 3-21. *Calcium fraction in exchanger (in %) in the buffer at different times (0, 1, 10 and 20 years) obtained for the heterogeneous case in which the contact area is equal to 20 cm².*

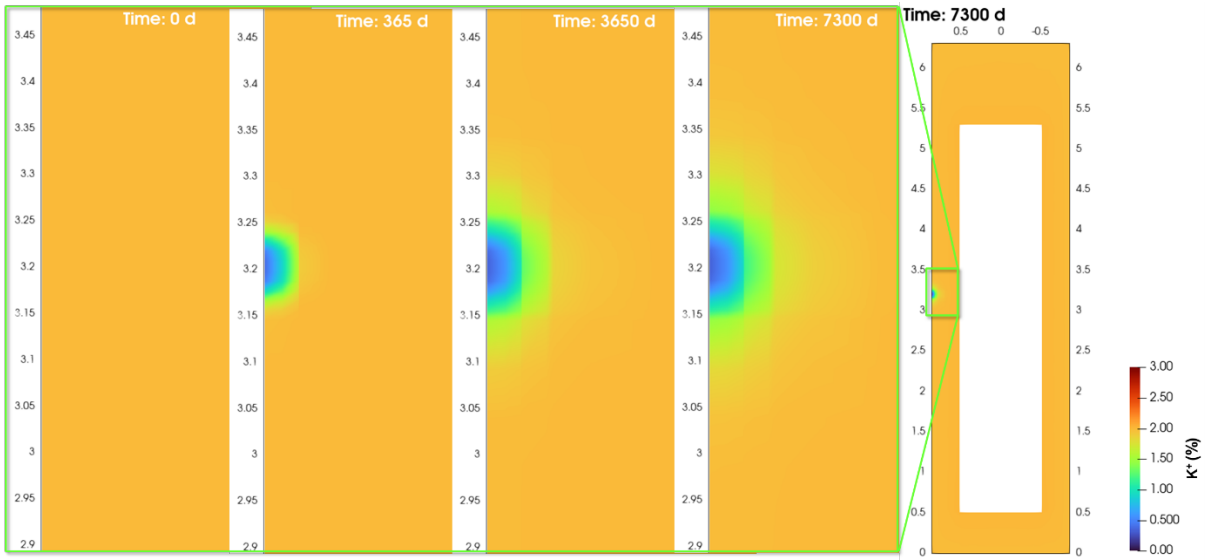

Figure 3-22. *Potassium fraction in exchanger (in %) in the buffer at different times (0, 1, 10 and 20 years) obtained for the heterogeneous case in which the contact area is equal to 20 cm².*

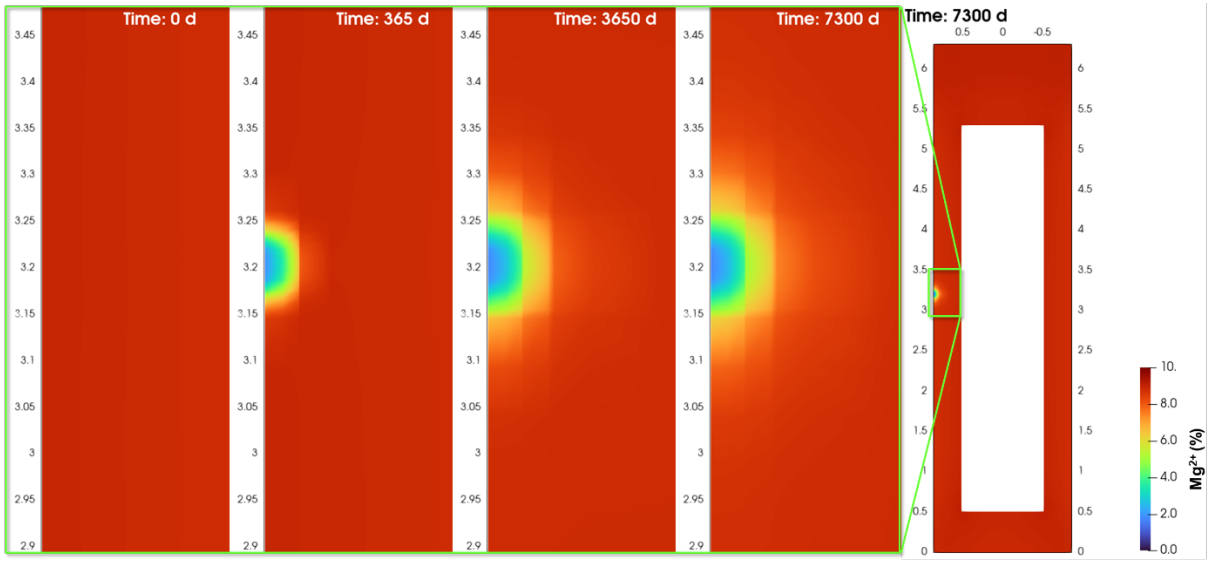

Figure 3-23. *Magnesium fraction in exchanger (in %) in the buffer at different times (0, 1, 10 and 20 years) obtained for the heterogeneous case in which the contact area is equal to 20 cm².*

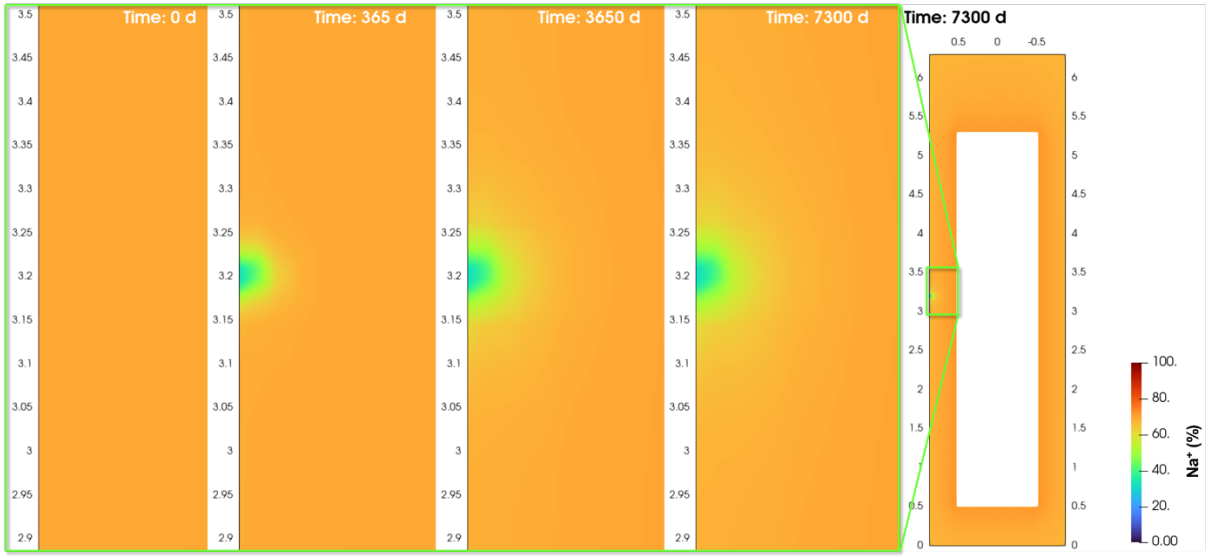

Figure 3-24. *Sodium fraction in exchanger (in %) in the buffer at different times (0, 1, 10 and 20 years) obtained for the heterogeneous case in which the contact area is equal to 5 cm².*

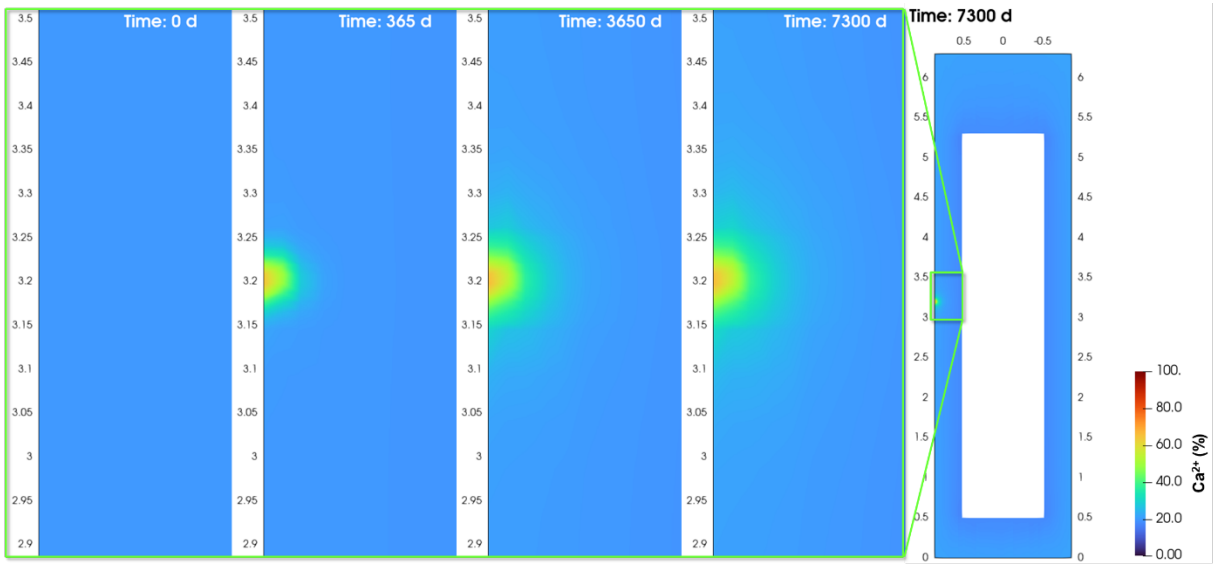

Figure 3-25. *Calcium fraction in exchanger (in %) in the buffer at different times (0, 1, 10 and 20 years) obtained for the heterogeneous case in which the contact area is equal to 5 cm^2.*

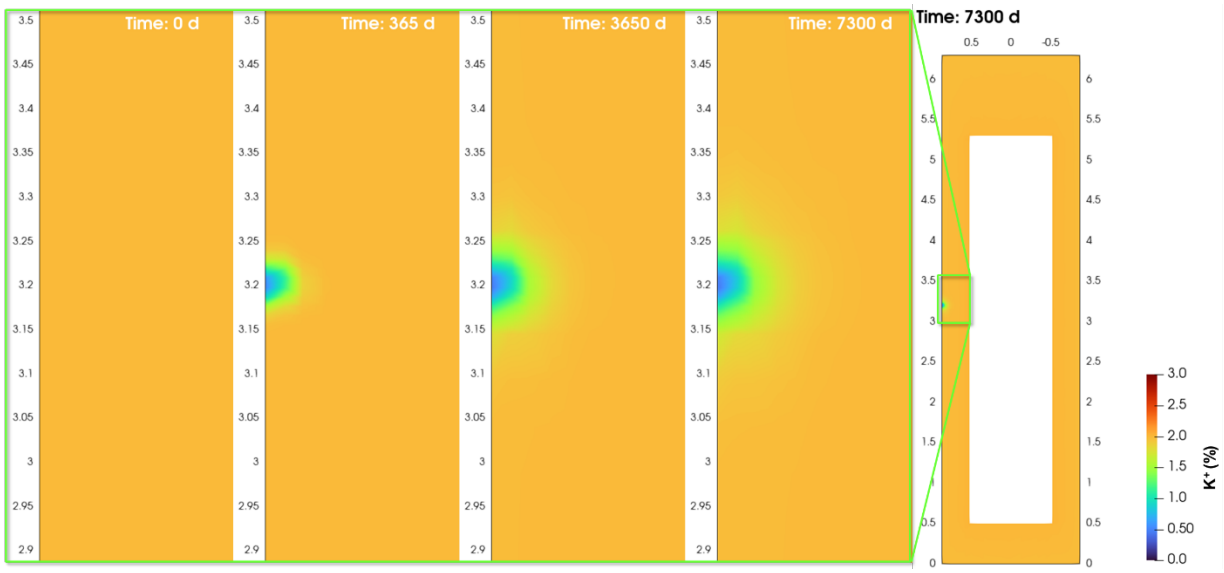

Figure 3-26. *Potassium fraction in exchanger (in %) in the buffer at different times (0, 1, 10 and 20 years) obtained for the heterogeneous case in which the contact area is equal to 5 cm^2.*

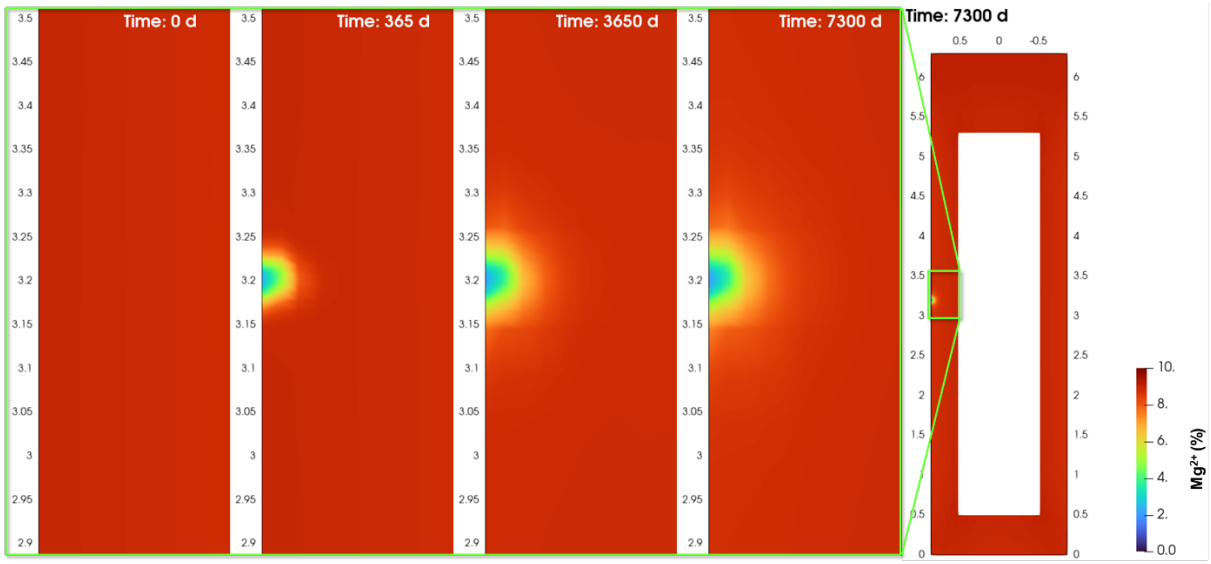

Figure 3-27. *Magnesium fraction in exchanger (in %) in the buffer at different times (0, 1, 10 and 20 years) obtained for the heterogeneous case in which the contact area is equal to 5 cm².*

Radial profiles of the cation exchange distribution at buffer mid-height are presented in Figure 3-28 and Figure 3-29 for the cases with a contact area of 20 and 5 cm², respectively. After 20 years, calcium replaces sodium as the major cation in the outer 5 cm of the buffer closest to the rock in the case with a contact area of 20 cm², while for the case with a contact area equal to 5 cm², this substitution only occurs in the outer 2.5 cm. Potassium and magnesium proportions decrease at the buffer-rock interface for both cases. The cation exchange front reaches 15-20 cm into the buffer after 20 years and slows down considerably with time.

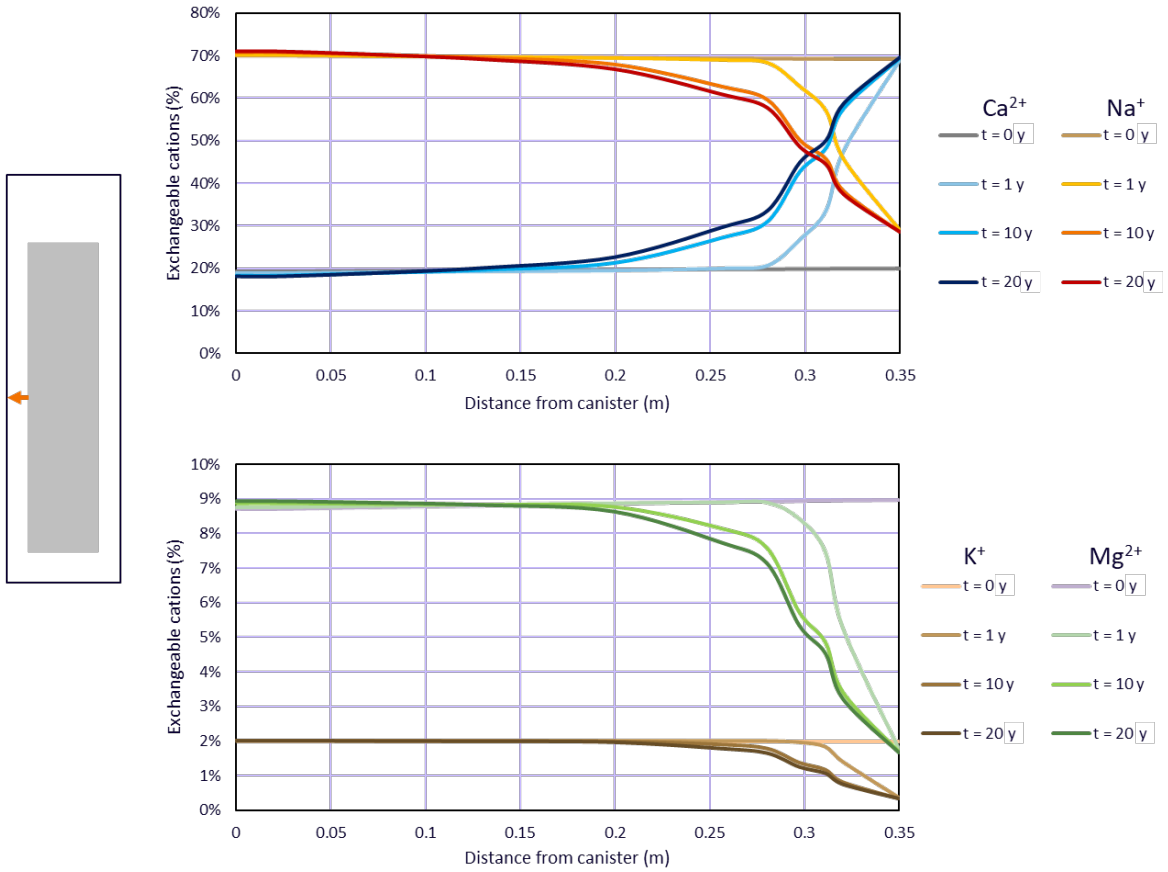

Figure 3-28. *Radial profiles, at buffer mid-height, of the exchangeable cation composition (in %) obtained for the heterogeneous case in which the contact area is equal to 20 cm² at different times (0, 1, 10 and 20 years).*

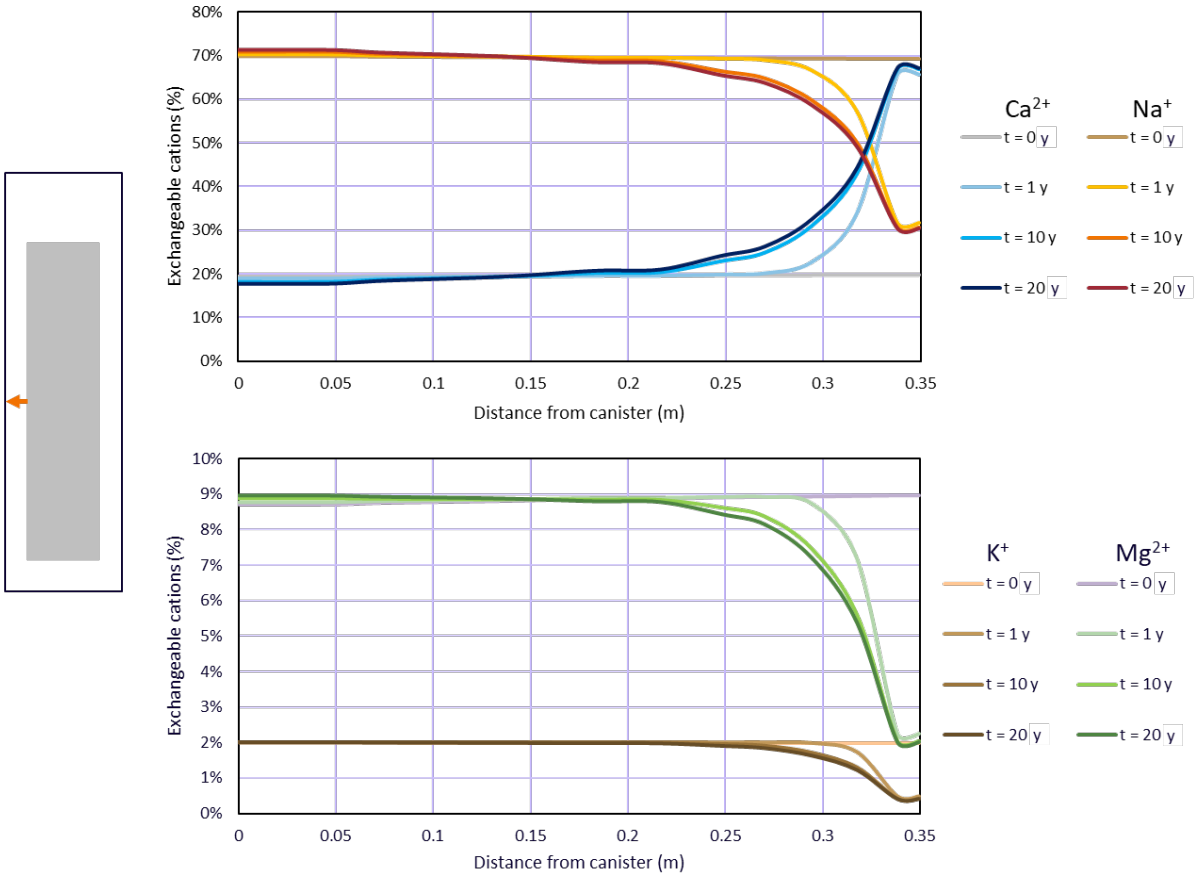

Figure 3-29. *Radial profiles, at buffer mid-height, of the exchangeable cation composition (in %) obtained for the heterogeneous case in which the contact area is equal to 5 cm^2 at different times (0, 1, 10 and 20 years).*

3.2.2 Fracture cases

The cases test the scenario of a water-conducting fracture crossing the buffer. The models include the volume of the rock matrix and a fracture that crosses the deposition hole at its mid-height. In a first stage, conservative transport modelling has been carried out to evaluate which fracture transmissivities are of interest (intermediate behaviour between the base line model case and the rock-limited diffusion case). Five cases that cover a range of fluid velocities from 10^{-9} to 10^{-5} m/s in the fracture have been simulated. Figure 3-30 shows the concentration profile of a tracer (Tr2) that diffuses out of the buffer for each case after 365, 700, 3650 and 7300 days, respectively. In the cases with lower velocities (10^{-9} and 10^{-8} m/s) tracer concentrations increase in the fracture near the buffer and the main transport mechanism is diffusion. In the cases of higher fluid velocities (10^{-6} and 10^{-5} m/s), the advective term plays an important role and almost all of the out-diffused tracer is transported farther away from the buffer. In the intermediate case, a tracer plume is formed in the direction of the fracture flow.

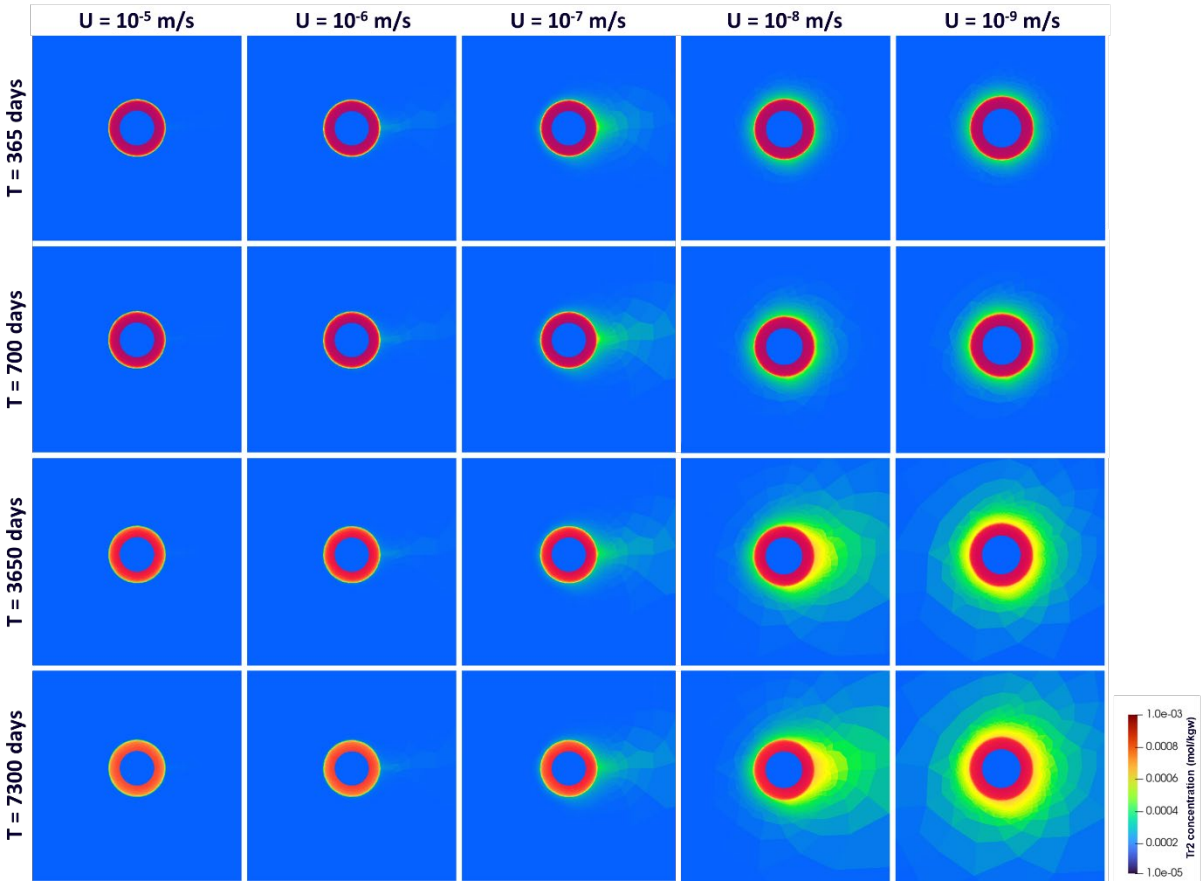

Figure 3-30. *Out-diffused tracer (Tr2) concentration (in mol/kgw) in a horizontal section of the fracture and buffer at different times for each conservative fracture case.*

Figure 3-31 shows the equivalent amount of in-diffused solution into the bentonite buffer for the cases with the different fracture flow velocities. The results show that the advective flow in the fracture can significantly increase the interaction between the buffer and the fracture. In the cases with low velocities, the main solute transport mechanism in the fracture is diffusion and the amount of in-diffused solution into the buffer is of 0.075 m^3. In the cases with higher flowrates, both diffusion and advection played an important role, and about 0.14 m^3 have diffused in after 20 years. In any case, the contact area between the fracture and the buffer is only a fraction of its total surface and the interaction is very low as compared to the baseline model (right plot in Figure 3-31).

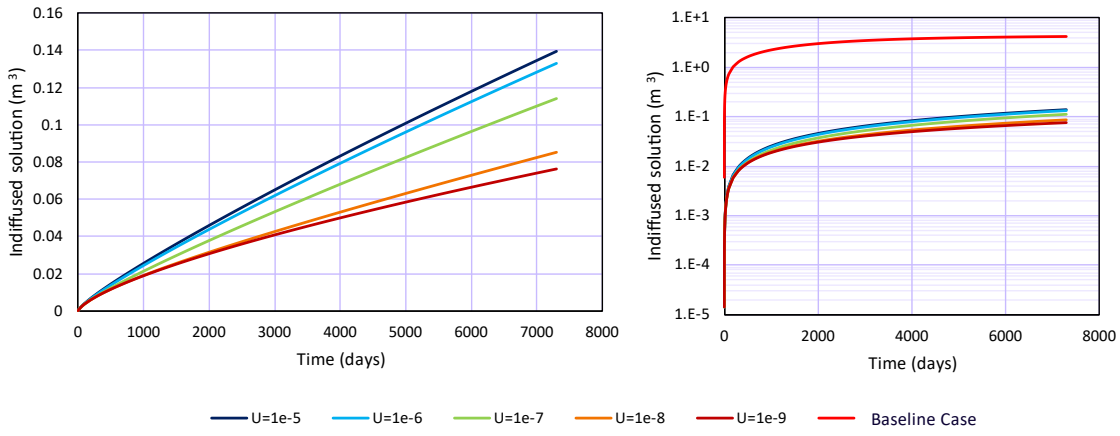

Figure 3-31. *Temporal evolution of the equivalent in-diffused groundwater into to the buffer, in m^3, obtained for the different fracture cases. The graph on the right compares the results to those obtained with the baseline model.*

In view of these results, reactive transport modelling has been carried out with the cases that consider flow velocities in the fracture of 10^{-8} and 10^{-6} m/s, as they are representative of two opposite cases: diffusive solute transport in the fracture and diffusive-advective transport in the fracture.

Figure 3-32 and Figure 3-33 show the (Tr1) tracer concentration in a vertical cross section of the entire model geometry for the two fracture cases. These figures illustrate how only the bentonite buffer zone close to the fracture is affected in terms of tracer concentrations. Concentrations in the fracture are significantly higher in the case with high fracture velocity. In the case of 10^{-8} m/s, a plume can be observed in the fracture with low concentrations of Tr1 tracer due to the interaction with the buffer. The contact between the rock matrix and the buffer has a very small effect on the buffer, but results in a significant tracer decrease in the rock. This effect is caused by the fact that the rock matrix has much lower porosity than the buffer.

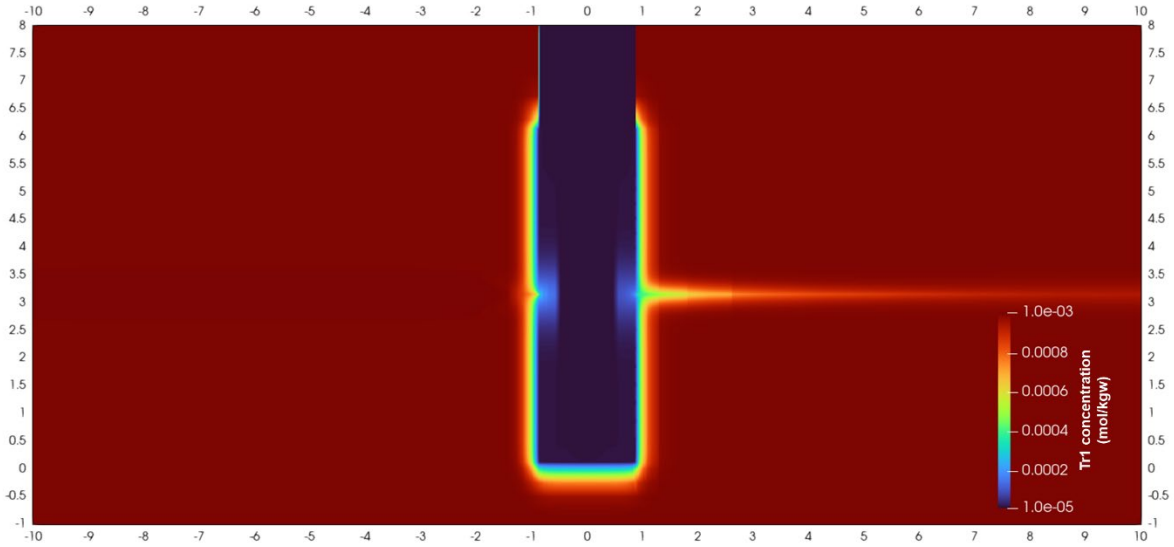

Figure 3-32. *Concentration of tracer Tr1 (in mol/kgw) in a vertical cross-section of the model after 20 years for the case with a fracture flow velocity equal to 10^{-8} m/s.*

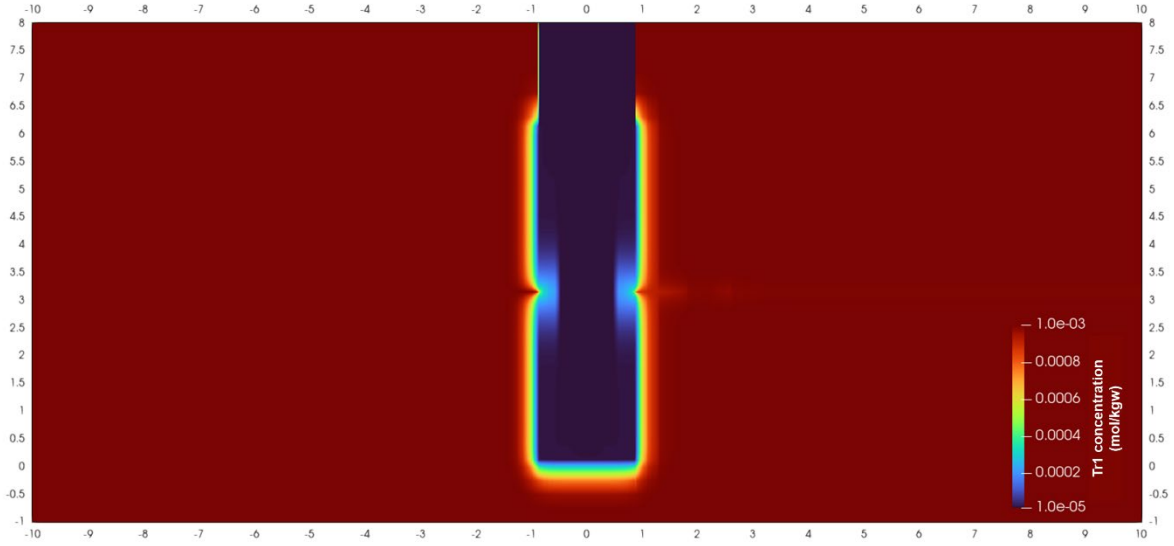

Figure 3-33. *Concentration of tracer Tr1 (in mol/kgw) in a vertical cross-section of the model after 20 years for the case with a fracture flow velocity equal to 10^{-6} m/s.*

Anhydrite precipitates slightly next to the canister (heater) and around the inlet area in the buffer (Figure 3-34 and Figure 3-35 for 10^{-8} and 10^{-6} m/s, respectively), as observed in the heterogenous cases. Anhydrite precipitation takes place next to the canister due to the temperature gradient in this area and next to the interface with the fracture due to the incoming calcium that reacts with the sulphate in the buffer (Figure 3-36 and Figure 3-37).

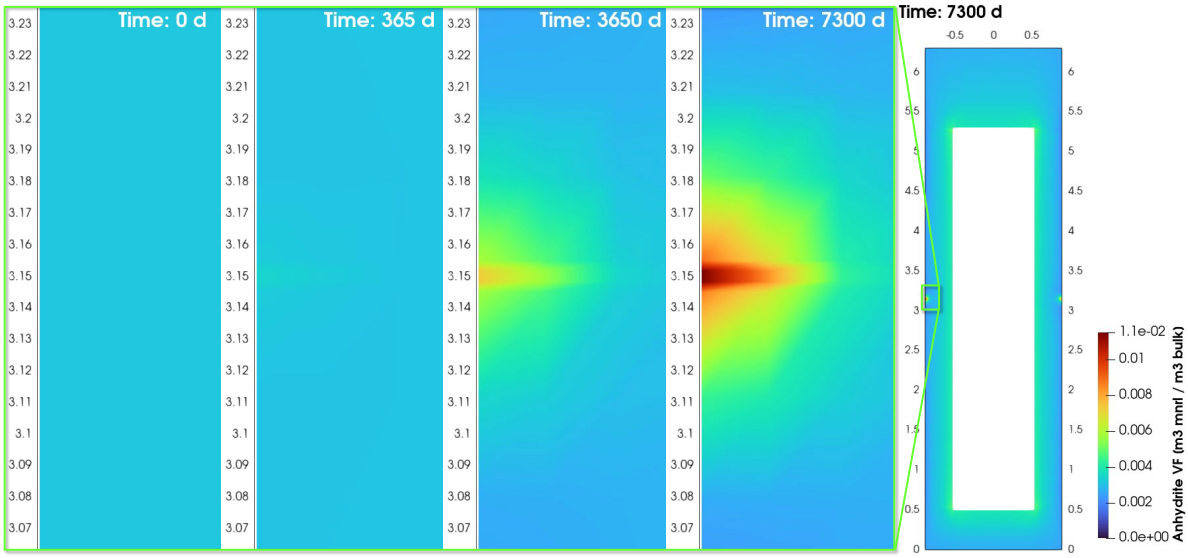

Figure 3-34. *Volume fraction of anhydrite in the buffer at different times (0, 1, 10 and 20 years) obtained for the fracture case with a fracture flow velocity of 10^{-8} m/s.*

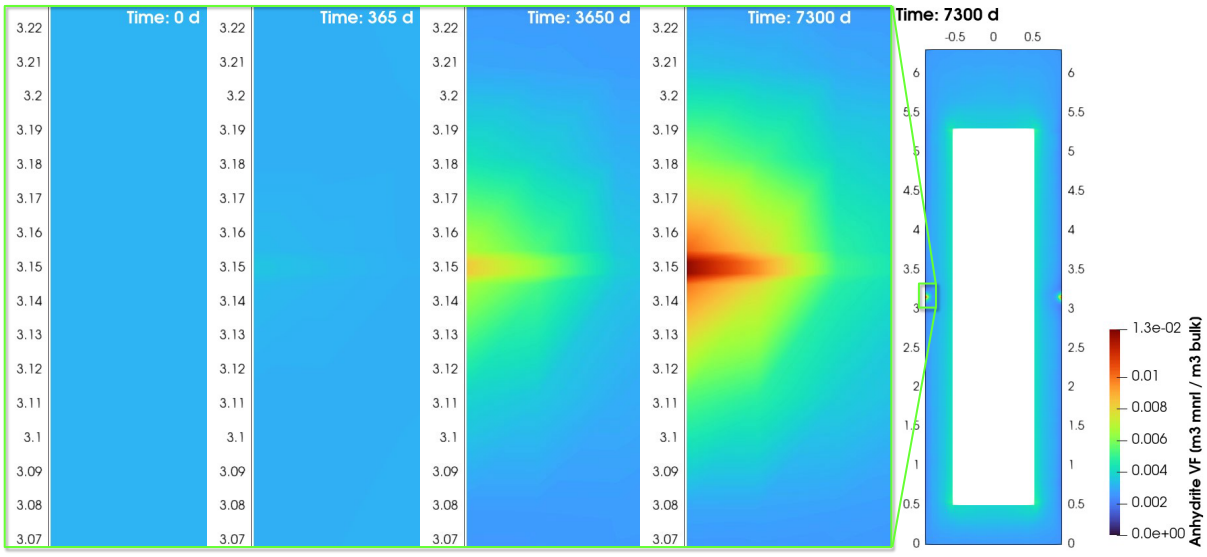

Figure 3-35. *Volume fraction of anhydrite in the buffer at different times (0, 1, 10 and 20 years) obtained for the fracture case with a fracture flow velocity of 10^{-6} m/s.*

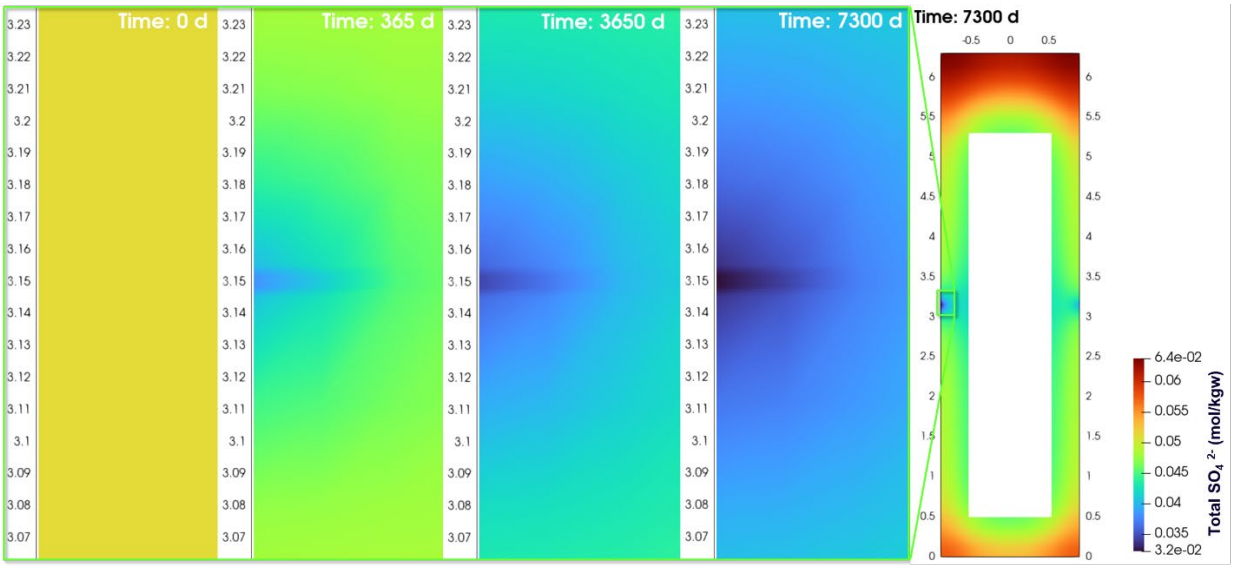

Figure 3-36. *Aqueous sulphate concentration (in mol/kgw) in the buffer at different times (0, 1, 10 and 20 years) obtained for the fracture case with a fracture flow velocity of 10^{-8} m/s.*

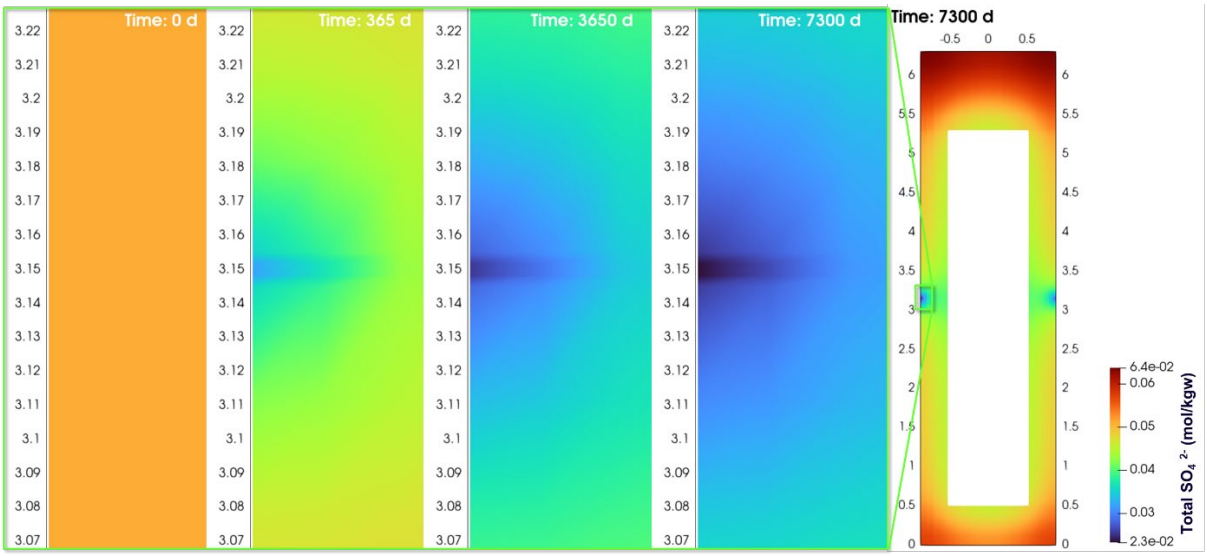

Figure 3-37. *Aqueous sulphate concentration (in mol/kgw) in the buffer at different times (0, 1, 10 and 20 years) obtained for the fracture case with a fracture flow velocity of 10^{-6} m/s.*

Regarding cation exchange, Figure 3-38 shows the temporal evolution of the four cations at point A (see Figure 3-6). The exchange reactions take place faster at the beginning of the simulation (until 2 years), especially in the case of a fracture velocity equal to 10^{-6} m/s. After that, the amount of each cation is quasi-constant. In both cases, sodium remains the major cation with fractions of 55-62 %.

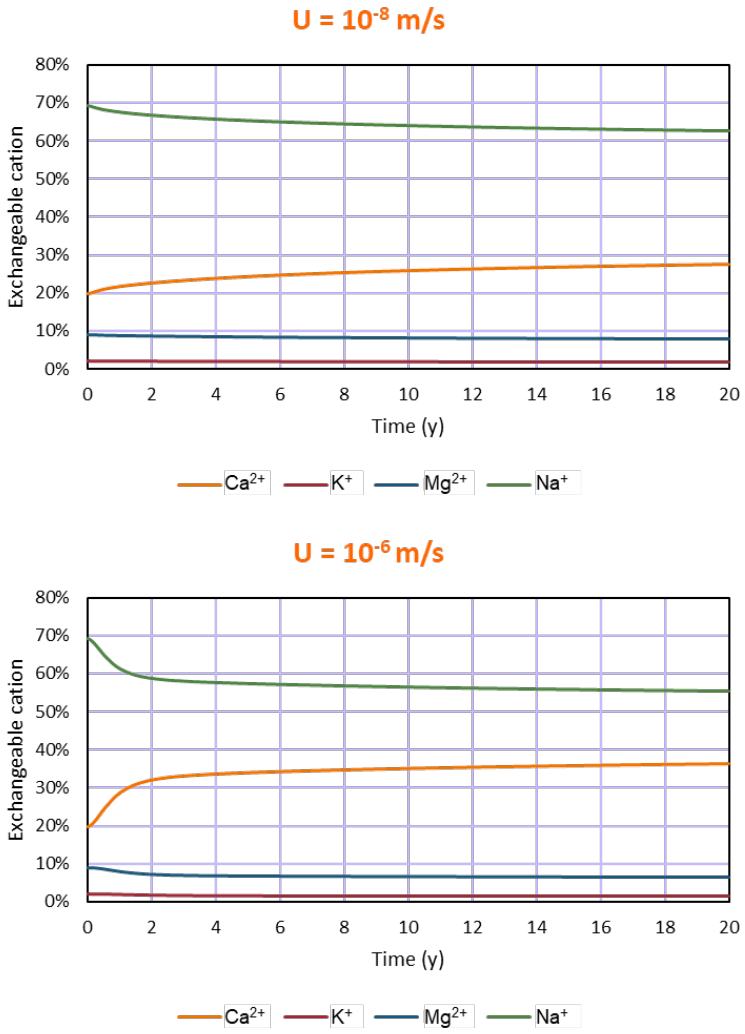

Figure 3-38. *Temporal evolution of the cation exchange composition (in %) in the buffer 2 cm from the buffer-fracture interface (point A in Figure 3-6) obtained for both fracture cases, 10^{-8} m/s (top) and 10^{-6} m/s (bottom).*

The spatial distribution of each cation next to the interface between the bentonite buffer and the fracture at different times (0, 1, 10 and 20 years) is shown for 10^{-8} m/s in Figure 3-39 to Figure 3-42 and for 10^{-6} m/s in Figure 3-43 to Figure 3-46. In both cases, the cation exchange composition changes mainly next to the fracture and the surrounding 10-20 cm of buffer. Smaller changes can be observed at the interface between the buffer and the rock matrix, as solute transport is more restricted in this area.

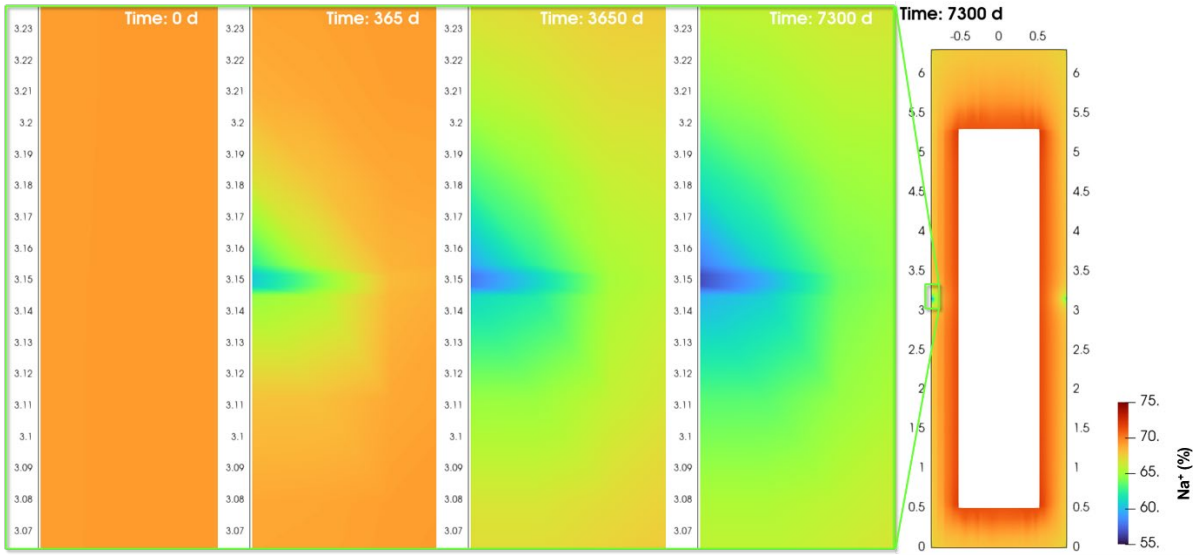

Figure 3-39. *Sodium fraction in exchanger (in %) in the buffer at different times (0, 1, 10 and 20 years) obtained with a fracture flow velocity equal to 10^{-8} m/s.*

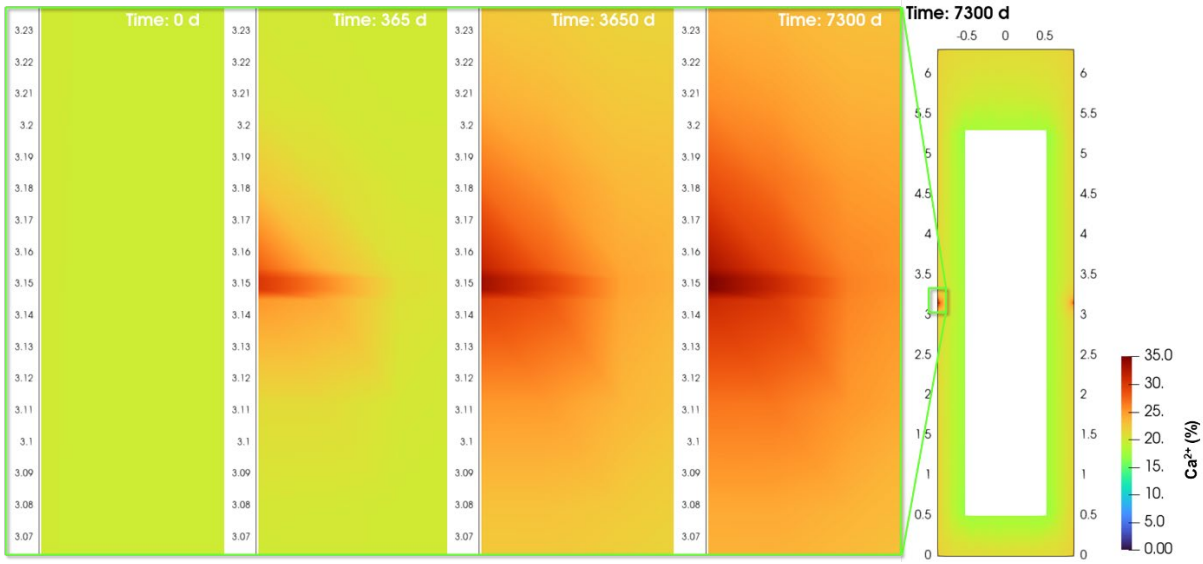

Figure 3-40. *Calcium fraction in exchanger (in %) in the buffer at different times (0, 1, 10 and 20 years) obtained with a fracture flow velocity equal to 10^{-8} m/s.*

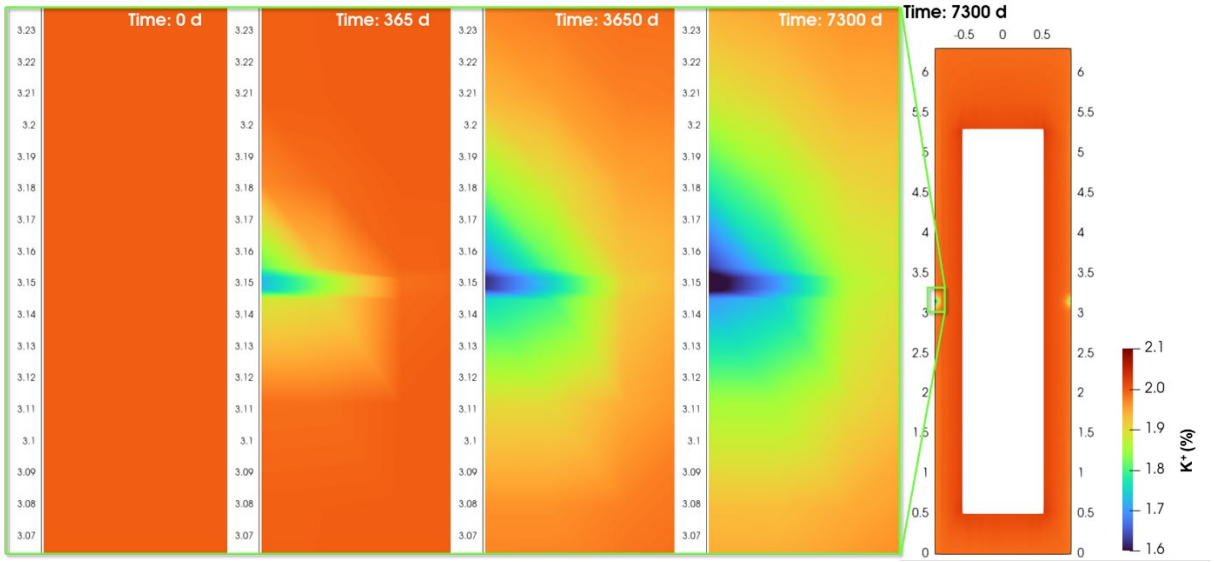

Figure 3-41. *Potassium fraction in exchanger (in %) in the buffer at different times (0, 1, 10 and 20 years) obtained with a fracture flow velocity equal to 10^{-8} m/s.*

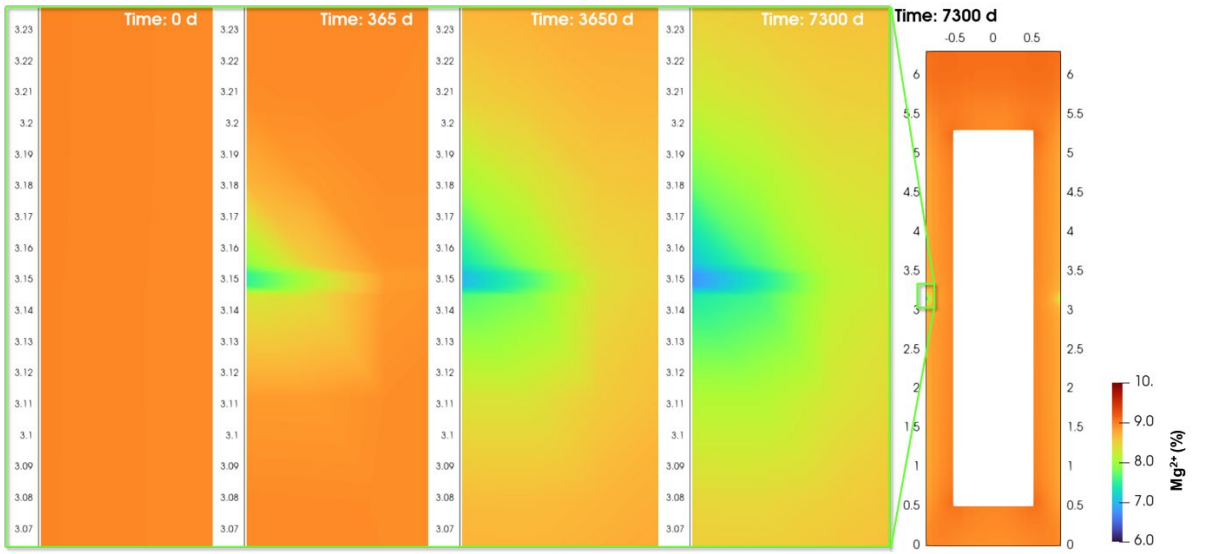

Figure 3-42. *Magnesium fraction in exchanger (in %) in the buffer at different times (0, 1, 10 and 20 years) obtained with a fracture flow velocity equal to 10^{-8} m/s.*

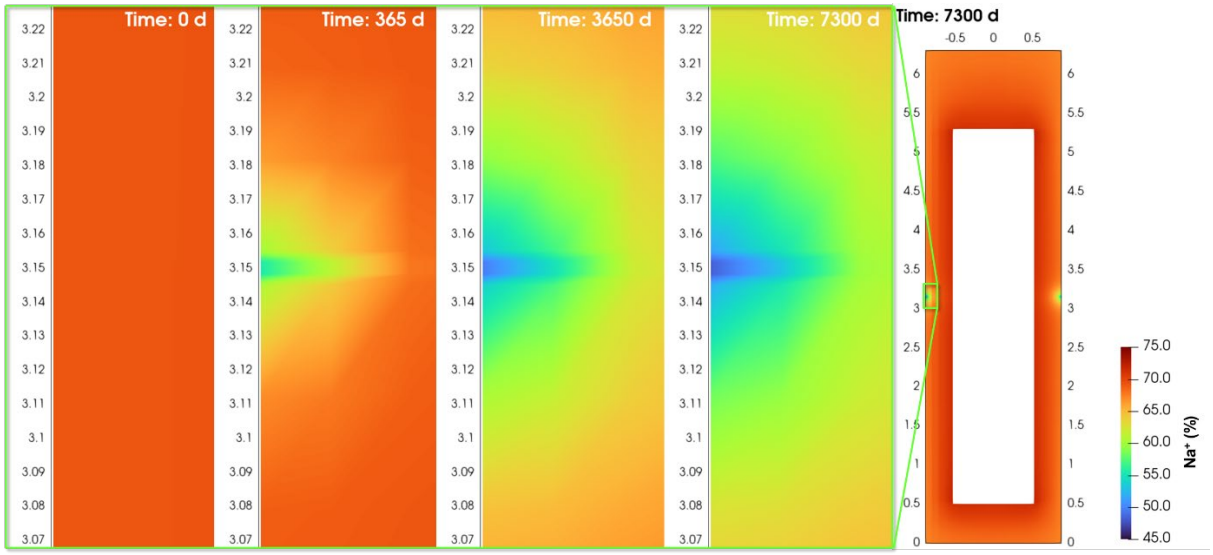

Figure 3-43. *Sodium fraction in exchanger (in %) in the buffer at different times (0, 1, 10 and 20 years) obtained with a fracture flow velocity equal to 10^{-6} m/s.*

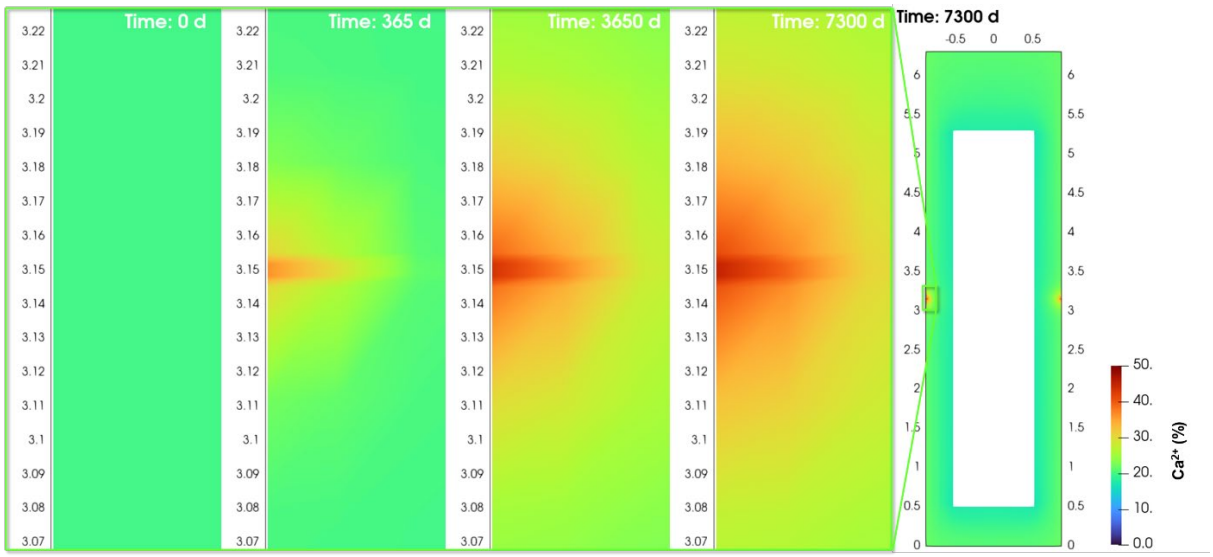

Figure 3-44. *Calcium fraction in exchanger (in %) in the buffer at different times (0, 1, 10 and 20 years) obtained with a fracture flow velocity equal to 10^{-6} m/s.*

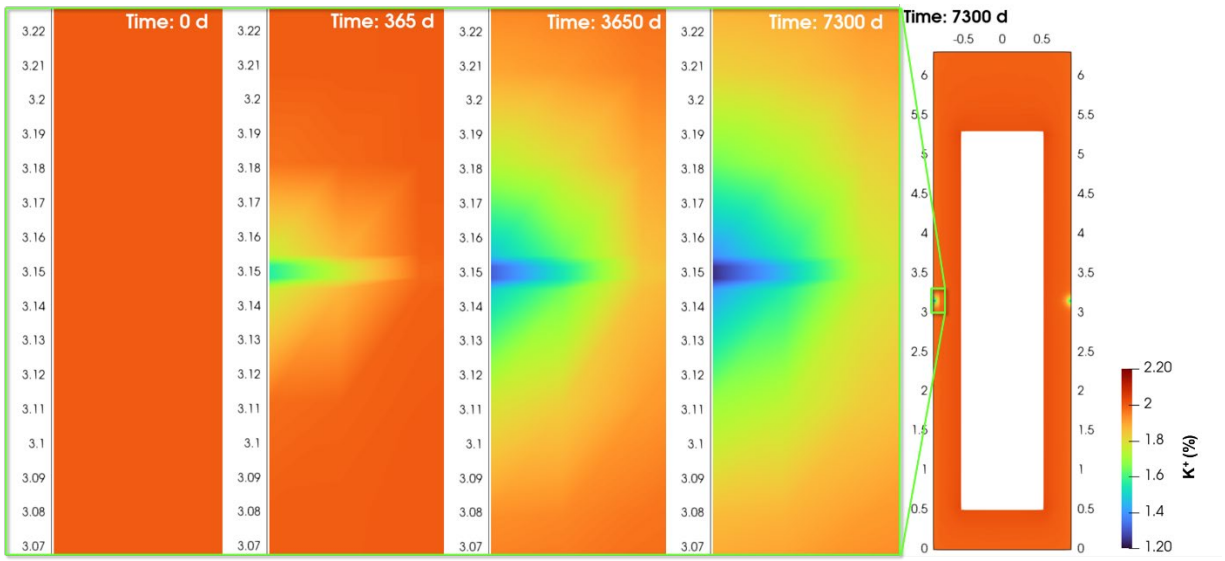

Figure 3-45. *Potassium fraction in exchanger (in %) in the buffer at different times (0, 1, 10 and 20 years) obtained with a fracture flow velocity equal to 10^{-6} m/s.*

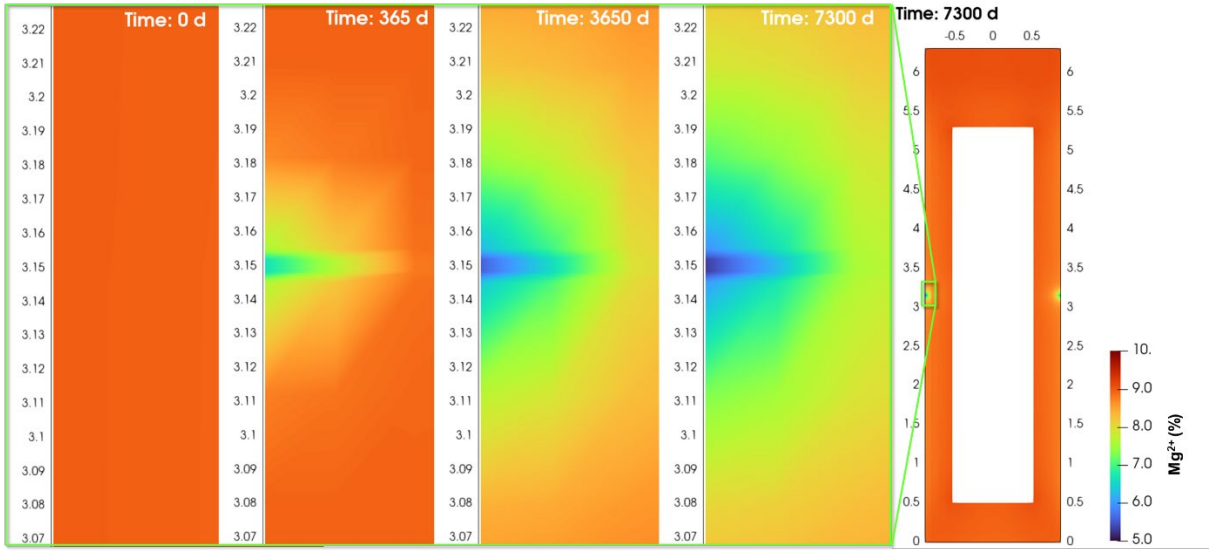

Figure 3-46. *Magnesium fraction in exchanger (in %) in the buffer at different times (0, 1, 10 and 20 years) obtained with a fracture flow velocity equal to 10^{-6} m/s.*

Figure 3-47 and Figure 3-48 show the radial distribution of the fractions occupied by each exchangeable cation for the two cases studied. After 20 years, a high flow velocity in the fracture increases the spatial extent (from 7.5 to 15 cm) of significant changes in the composition of the exchanger. However, sodium remains the main cation in both cases.

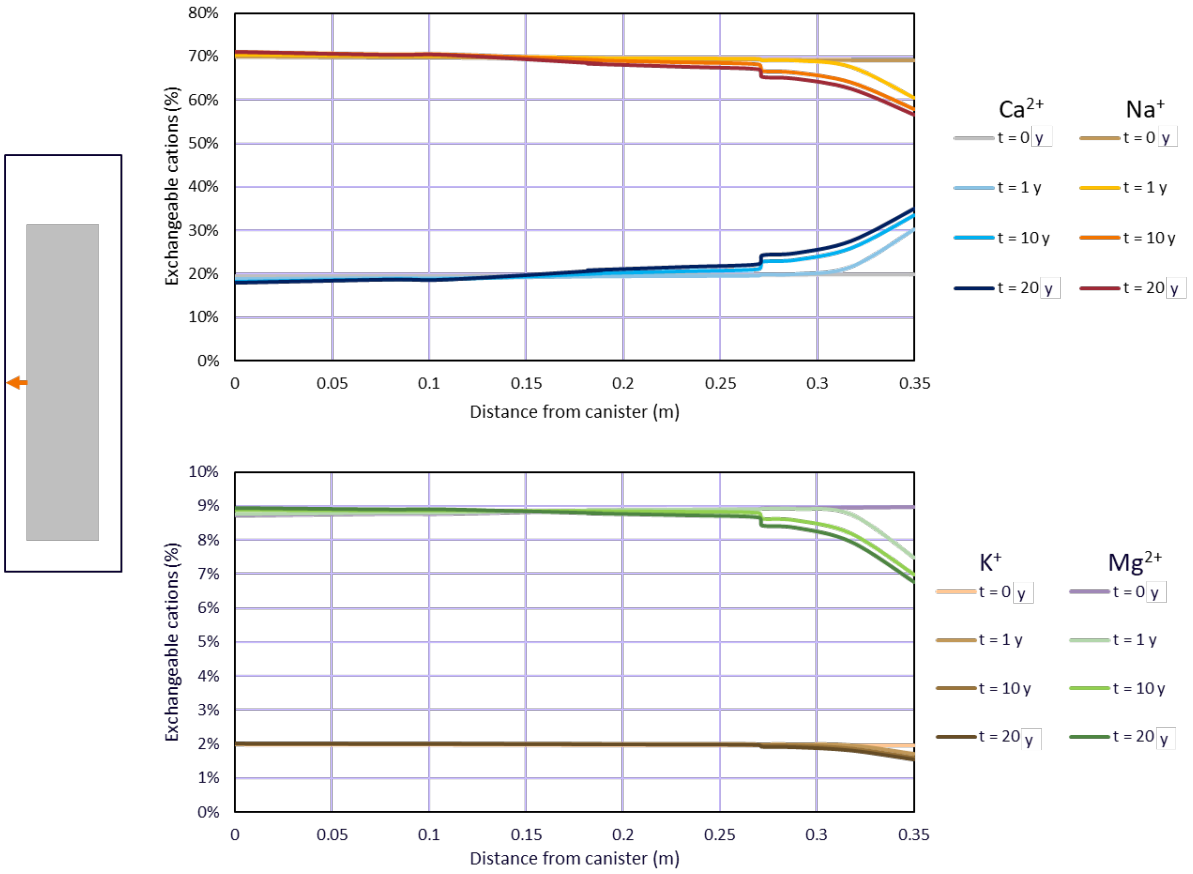

Figure 3-47. *Radial profiles, at buffer mid-height, of the exchangeable cation composition (in %) obtained with a fracture flow velocity equal to 10^{-8} m/s.*

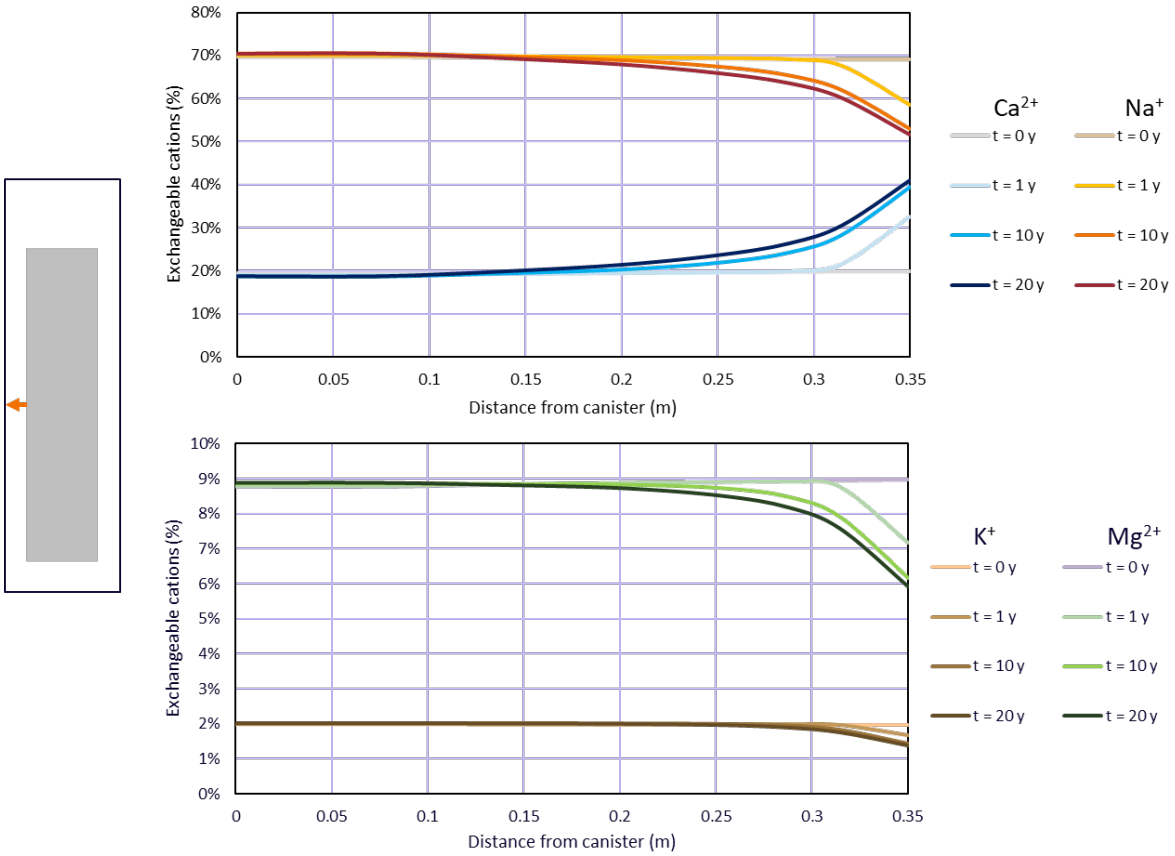

Figure 3-48. *Radial profiles, at buffer mid-height, of the exchangeable cation composition (in %) obtained with a fracture flow velocity equal to 10^{-6} m/s.*

3.2.3 Rock-limited diffusion

This sensitivity case studies a scenario in which the interaction between the buffer and the rock is limited by the transport properties of an intact rock matrix without fractures. In this case, the buffer is fully surrounded by rock matrix with low porosity and a low effective diffusion coefficient.

The evolution of the Tr1 tracer concentration in the buffer is displayed in Figure 3-49. The inflow of tracer is two orders of magnitude lower than in the baseline case (note the colour scale in Figure 3-49) due to the low diffusive properties of the rock matrix. The same effect can be observed in Figure 3-50, where the amount of equivalent in-diffused solution is compared to that of the baseline model.

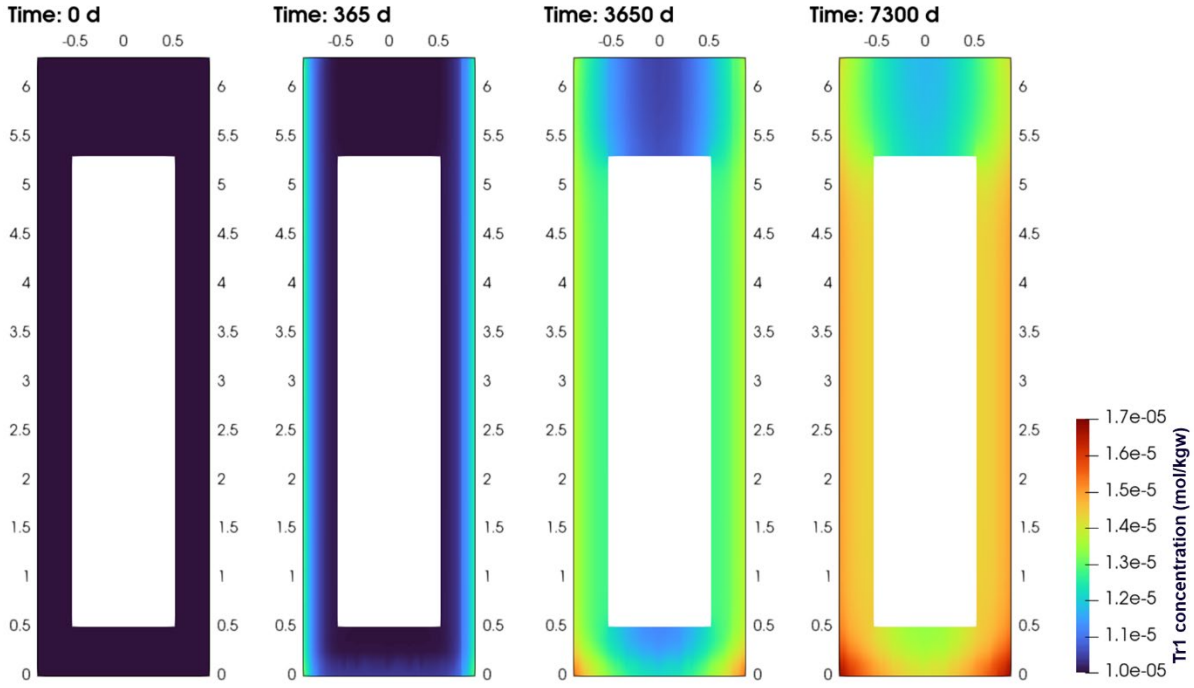

Figure 3-49. *Concentration of tracer Tr1 in the buffer (in mol/kgw) at different times (0, 1, 10 and 20 years) obtained for the rock-limited diffusion case.*

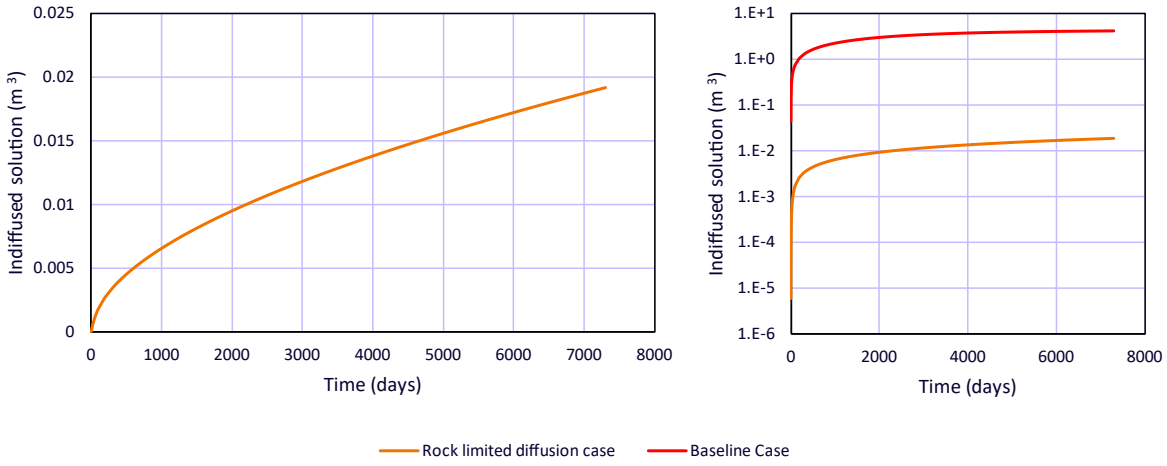

Figure 3-50. *Temporal evolution of the equivalent in-diffused groundwater into to the buffer, in m^3, obtained for the rock-limited diffusion case. The graph on the right compares the results to those obtained with the baseline model.*

Regarding the dissolution/precipitation of anhydrite, a similar behaviour to the baseline model has been observed here. Anhydrite dissolves close to the buffer-rock interface (Figure 3-51) due to sulphate outflow (Figure 3-52) and precipitates slightly close to the canister. In this sensitivity case, anhydrite is not fully dissolved at the buffer-rock interface, as was the case in the baseline model. Also, variations in sulphate concentrations are considerably lower (compare Figure 3-5 with Figure 3-52).

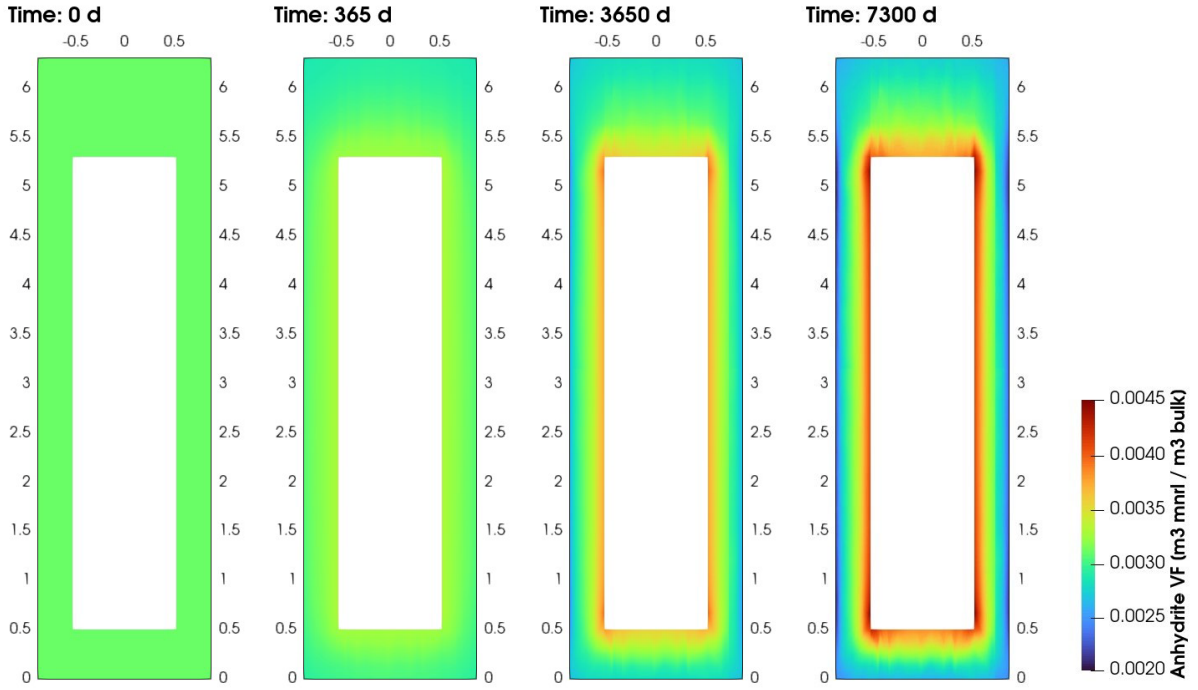

Figure 3-51. *Volume fraction of anhydrite in the buffer at different times (0, 1, 10 and 20 years) obtained for the rock-limited diffusion case.*

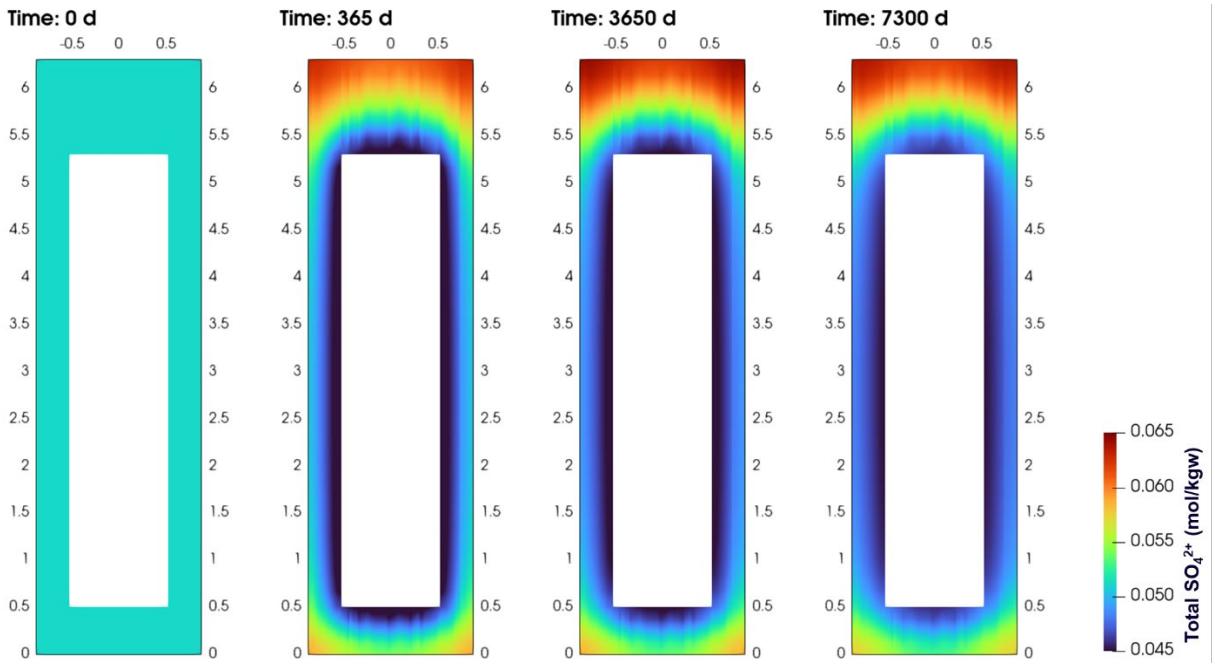

Figure 3-52. *Aqueous sulphate concentration (in mol/kgw) in the buffer at different times (0, 1, 10 and 20 years) obtained for the rock-limited diffusion case.*

The cation exchange reactions taking place in this sensitivity case are very limited. In fact, the temperature gradient caused by the canister (heater) seems to have a larger effect than the geochemical interaction between the buffer and the rock matrix. Figure 3-53 shows the evolution of the cation exchange composition in the buffer at point A (see Figure 3-6), which presents variations of only a few % in 20 years. The changes in cation exchange distribution are better observed in the figures of the spatial distribution of cations in the exchanger: Figure 3-54 to Figure 3-57. Note that the colour scale has been adjusted to visualize the small changes in the fraction of cations.

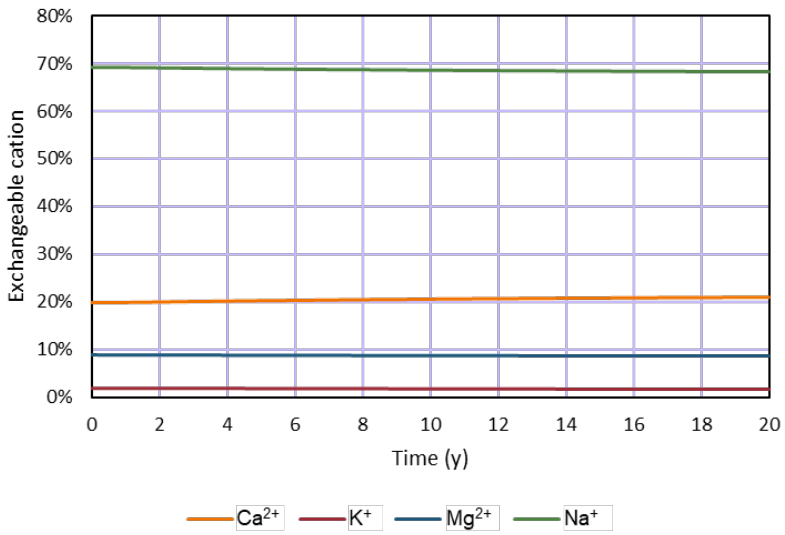

Figure 3-53. *Temporal evolution of the cation exchange composition (in %) in the buffer 2 cm from the buffer-rock interface (point A in Figure 3-6) obtained for the rock-limited diffusion case.*

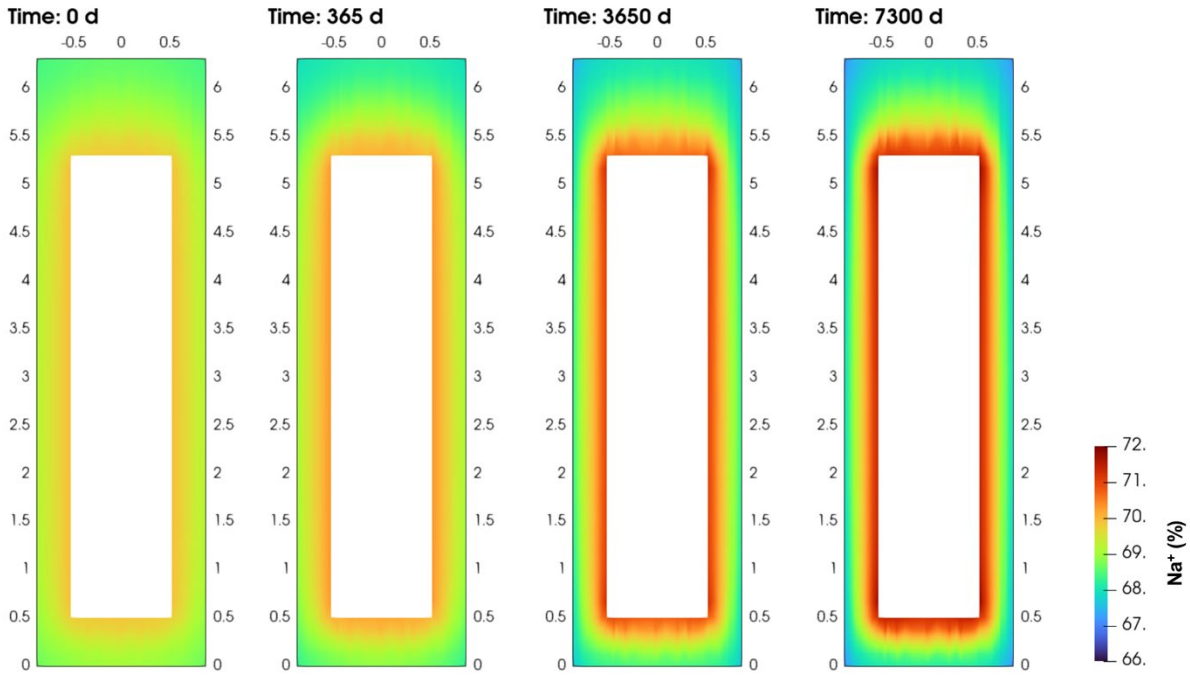

Figure 3-54. *Sodium fraction in exchanger (in %) in the buffer at different times (0, 1, 10 and 20 years) obtained for the rock-limited diffusion case.*

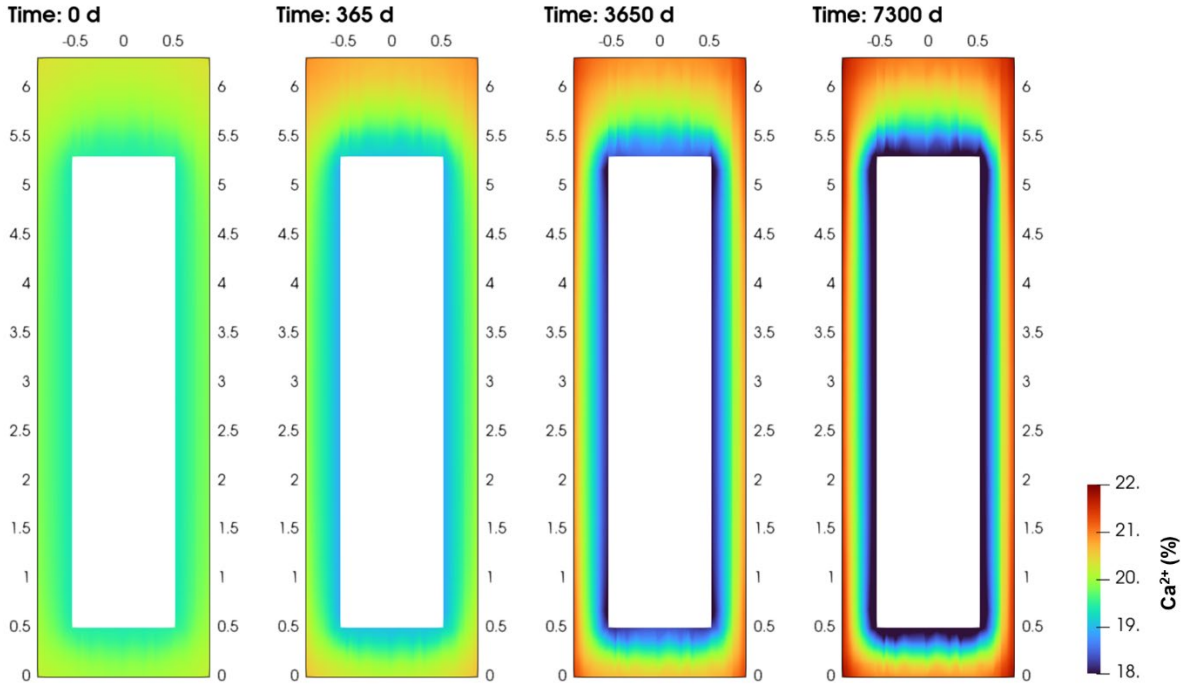

Figure 3-55. *Calcium fraction in exchanger (in %) in the buffer at different times (0, 1, 10 and 20 years) obtained for the rock-limited diffusion case.*

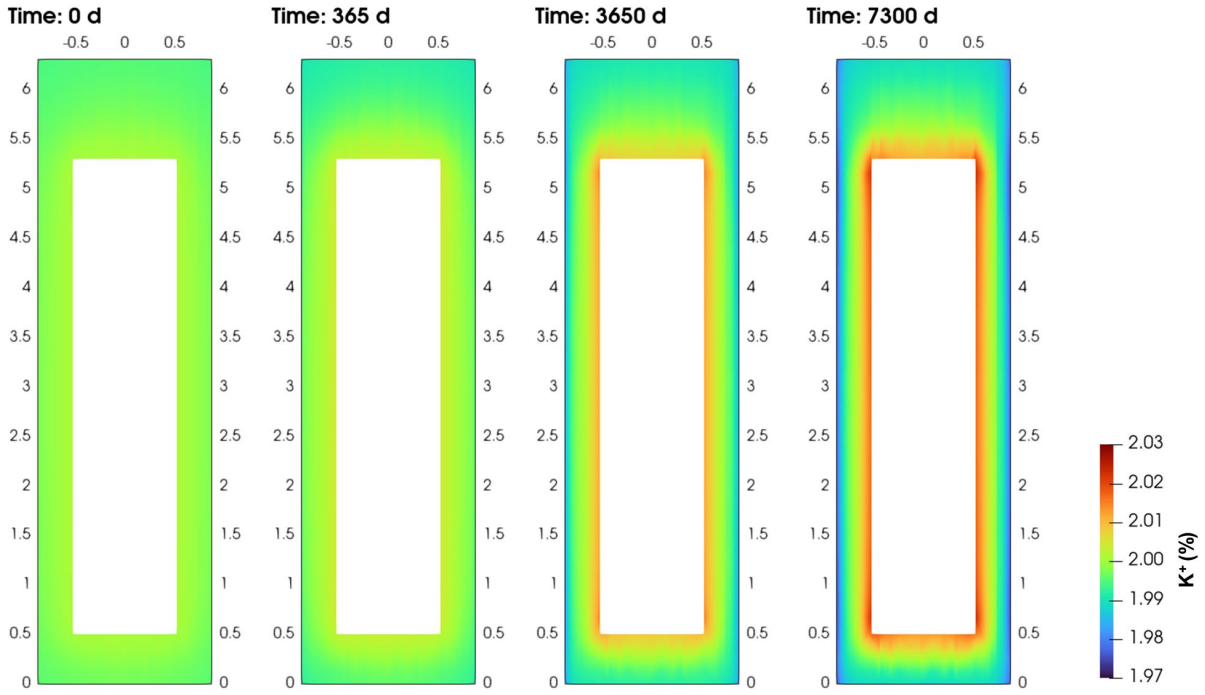

Figure 3-56. *Potassium fraction in exchanger (in %) in the buffer at different times (0, 1, 10 and 20 years) obtained for the rock-limited diffusion case.*

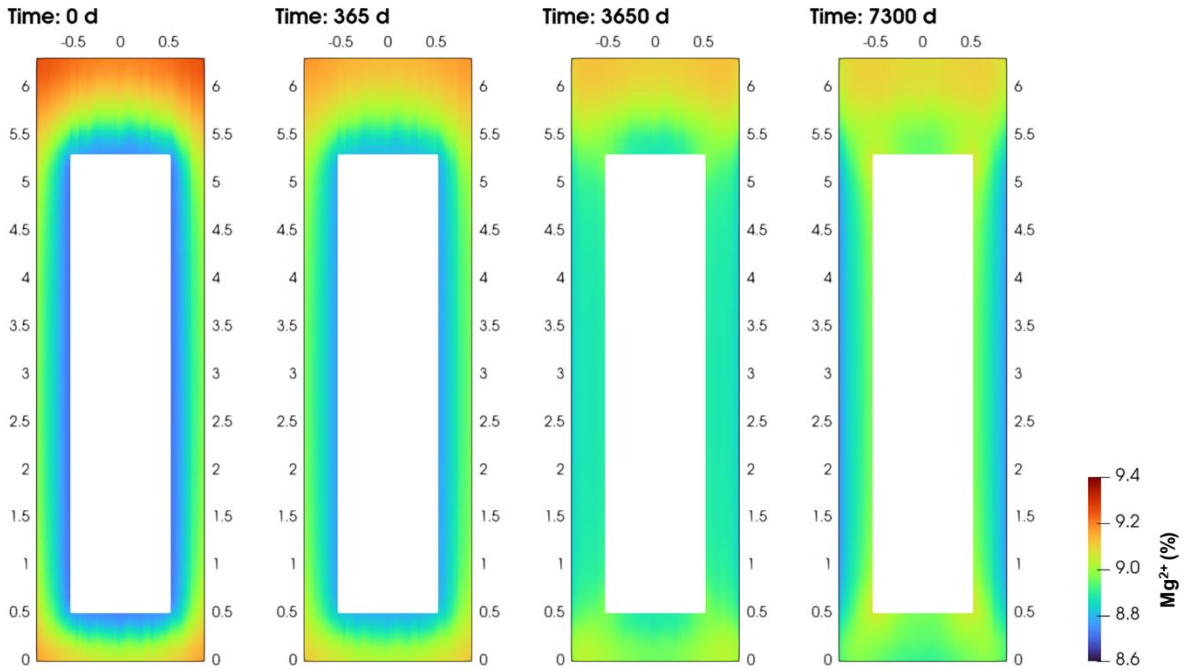

Figure 3-57. *Magnesium fraction in exchanger (in %) in the buffer at different times (0, 1, 10 and 20 years) obtained for the rock-limited diffusion case.*

Figure 3-58, finally, shows the radial profiles of cation composition obtained for this sensitivity case. Again, no significant changes are observed in the bentonite buffer.

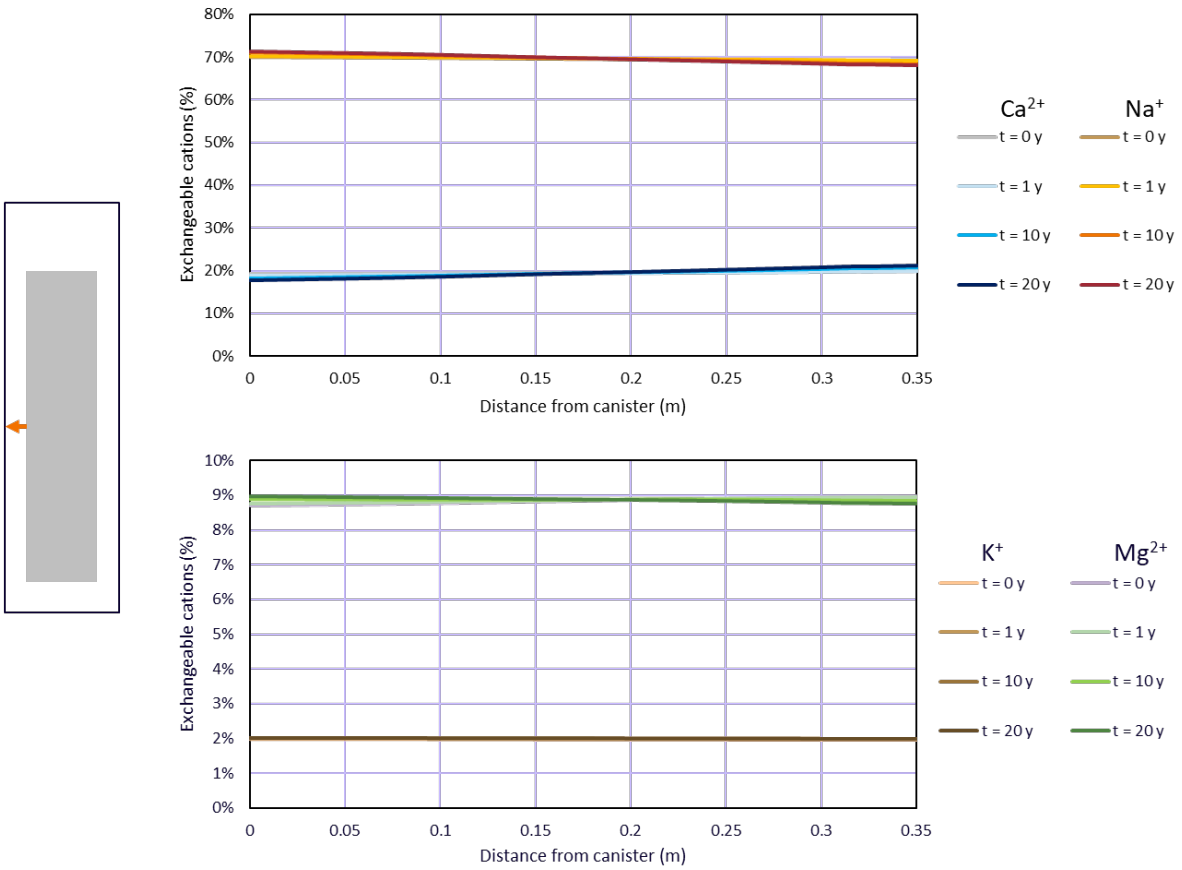

Figure 3-58. *Radial profiles of the exchangeable cation composition (in %) in the buffer at buffer mid-height obtained for the rock-limited diffusion case.*

4 Summary and conclusions

In the present work, several 3D reactive transport models of deposition hole 1 of the Prototype Repository experiment were implemented in PFLOTRAN to study the extent of cation exchange reactions expected to take place in the buffer. The models consider the temperature field developed due to the heater in the canister, which was verified with monitoring data. The models account for diffusive transport in the buffer and cation exchange reactions, as well mineral (anhydrite and calcite) reactions that may affect cation exchange under water-saturated, non-isothermal conditions. The granitic host rock surrounding the deposition hole is a heterogeneous porous medium that may include fractures or water-bearing features. In order to assess the effect of this uncertainty on the cation exchange evolution in the buffer, several modelling cases were developed, with differing representations of the host-rock. An upper bounding case, which maximizes the geochemical rock-buffer interaction, considered a fixed groundwater concentration at the rock-buffer interface. A lower bounding case, which indicates the minimum expected interaction, studied the buffer surrounded by rock matrix with low porosity and diffusivity. These cases simulated homogeneous conditions at the buffer surface. Additionally, four sensitivity cases considered the buffer in contact with water-bearing features and fractures.

In terms of mineral reactions, anhydrite was observed to precipitate next to the canister due to the temperature gradient. This also resulted in a small change in cation exchange composition in this area, where calcium fractions decreased in favour of the other cations. In the homogeneous models, the transport of sulphates in the buffer towards the rock resulted in anhydrite dissolution next to the buffer-rock interface. In the heterogeneous and fracture cases, on the other hand, limited outflow of sulphate and inflow of calcium resulted in anhydrite precipitation next to the contact areas. Calcite was included as a secondary phase in the models but was not observed to precipitate in any modelling case.

The diffusive mixing of groundwater and buffer porewater obtained for the different modelling cases is summarized in Figure 4-1, which shows the evolution of equivalent amount of in-diffused external solution for each case. The cases show great variability of rock-buffer interaction, in which the baseline case shows almost full replacement of the bentonite porewater by groundwater and the sensitivity cases show very little replacement. The more plausible cases are the heterogenous cases and those that consider fracture flow with low diffusive fluxes.

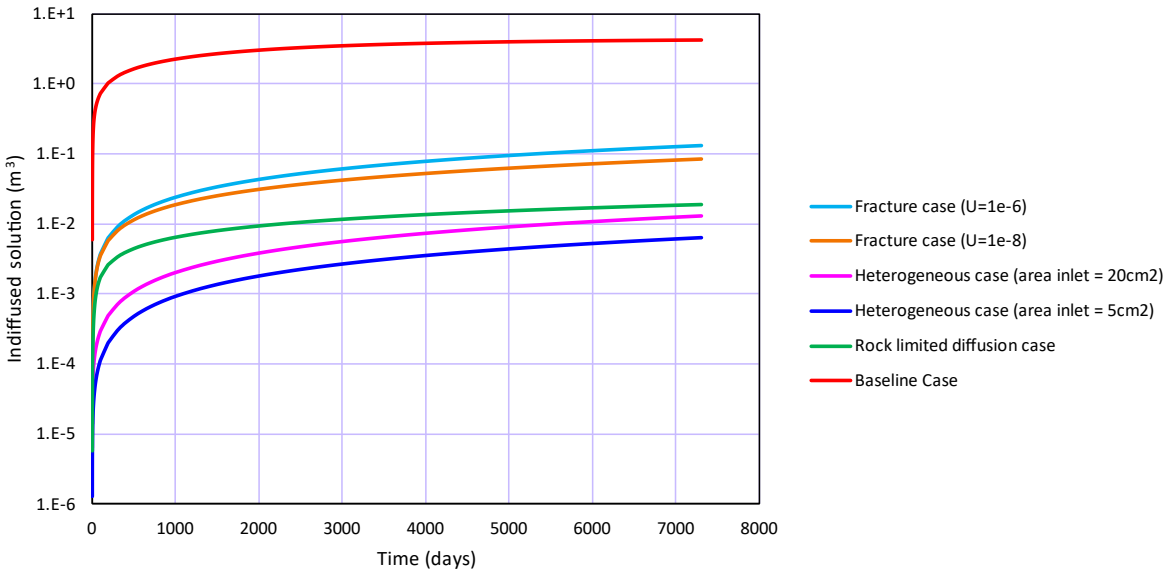

Figure 4-1. *Temporal evolution of the equivalent in-diffused groundwater into to the buffer, in m^3, obtained for the different modelling cases.*

The effect of the rock-buffer interaction on the cation exchange distribution is summarized in Figure 4-2, which shows the profile of calcium and sodium fractions in the buffer exchanger between the canister and the rock at the end of the experiment (20 years) obtained for the different cases. Note that for the homogeneous cases (baseline and rock-limited diffusion), this profile is representative of the whole buffer, whereas for the heterogenous cases (heterogeneous and fracture cases) it is valid only for the area directly next to the fracture or water-bearing feature. In general, the composition of the exchanger is expected to change between 1-2 % and 40-50 % in the outer part of the buffer (close to the rock), depending on the hydraulic conductivity and diffusive properties of the rock in that area. Cation exchange reactions are expected to take place within 5-10 cm from the buffer-rock interface. The baseline case predicts an extension of the region of cation exchange reactions, but it constitutes an unrealistic case that over-estimates buffer-rock interaction and cation exchange.

The general conclusion that can be drawn from the present work is that the transport properties of the host rock constitute a major limiting factor for cation exchange in the buffer, and that, as a result, the cation exchange composition in the buffer during the Prototype Repository experiment will be heterogeneously distributed and cation exchange reactions will likely take place mainly close to the buffer-rock interface (first few cm).

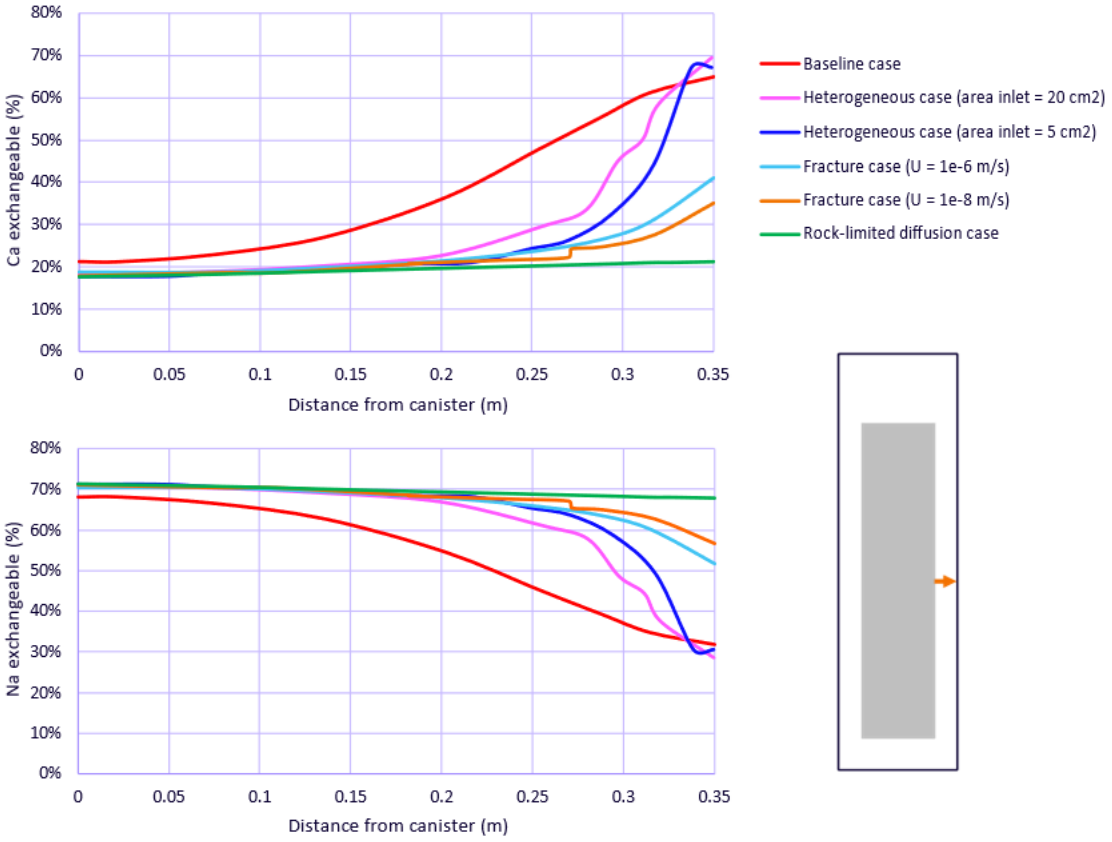

Figure 4-2. *Radial profiles of the calcium (top) and sodium (bottom) fractions in the exchanger (in %) after 20 years, obtained for the different modelling cases. The bottom right figure indicates the 1D line in the buffer where these profiles have been evaluated.*

References

SKB's (Svensk Kärnbränslehantering AB) publications can be found at www.skb.com/publications.

Bradbury M H, Baeyens B, 2002. Porewater chemistry in compacted re-saturated MX-80 bentonite: Physico-chemical characterisation and geochemical modelling. PSI Bericht 02–10, Villigen PSI and NTB 01–08, Nagra, Switzerland.

Coll A, Ribó R, Pasenau M, Escolano E, Perez JS, Melendo A, Monros A, Gárate J, 2018. GiD v.14 Customization Manual. CIMNE c2020, International Centre for Numerical Methods in Engineering, Spain.

Dohrmann R, Kaufhold S, 2014. Cation Exchange and Mineral Reactions Observed in MX 80 Buffer Samples of the Prototype Repository In Situ Experiment in Äspö, Sweden. Clays and Clay Minerals 62, 357–373. https://doi.org/10.1346/CCMN.2014.0620501

Giffaut G, Grivé M, Blanc P, Vieillard P, Colàs E, Gailhanou H, Gaboreau S, Marty N, Madé B, Duro L, 2014. Andra thermodynamic database for performance assessment: ThermoChimie. Applied Geochemistry 49, 225–236.

Goudarzi R, 2022. Prototype Repository – Sensor data report. Period 2001-09-17 to 2021-01-01. Report No 32. SKB P-21-28, Svensk Kärnbränslehantering AB.

Hammond G, Lichtner P, Mills R, 2014. Evaluating the performance of parallel subsurface simulators: An illustrative example with PFLOTRAN. Water Resources Research 50:1, 208–228.

Idiart A, Pekala M, Nardi A, Arcos D, 2012. Reactive transport modelling of the ABM experiment with Comsol Multiphysics. In International Meeting Clays in Natural & Engineered Barriers for Radioactive Waste, Montpellier, October 22–25 2012. Paris: INIS, 49–51.

Idiart A, Pękala M, Arcos D, 2014. Geochemical modelling of the ABM experiment at Äspö HRL. In 7th Mid-European Clay Conference, Dresden, September 16–19 2014. Dresden: MECC'14, 316.

Karnland O, Olsson S, Dueck A, Birgersson M, Nilsson U, Hernan-Håkansson T, Pedersen K, Nilsson S, Eriksen T-E, Rosborg B, 2009. Long-term test of buffer material at the Äspö Hard Rock Laboratory, LOT project. Final report on the A2 test parcel. SKB TR-09-29, Svensk Kärnbränslehantering AB.

Malmberg O, Åkeson M, 2022. Pre-dismantling Thermo-Hydraulic modelling of the buffer in the Prototype Repository. SKB P-22-17, Svensk Kärnbränslehantering AB.

Ohlsson Y, Neretnieks I, 1997. Diffusion data in granite, recommended values. SKB TR-97-20, Svensk Kärnbränslehantering AB.

Olsson S, Jensen V, Johannesson L E, Hansen E, Karnland O, 2013. Prototype Repository. Hydro-mechanical, chemical and mineralogical characterization of the buffer and tunnel backfill material from the outer section of the Prototype Repository. SKB TR-13-21, Svensk Kärnbränslehantering AB.

Ochs M, Talerico C, 2004. SR-Can. Data and uncertainty assessment. Migration parameters for the bentonite buffer in the KBS-3 concept. SKB Technical Report TR-04-18, Svensk Kärnbränslehantering AB.

Rhén I, Forsmark T, 2001. Äspö Hard Rock Laboratory. Prototype Repository Hydrogeology. Summary report of investigations before the operation phase. International Progress Report IPR-01-65, Svensk Kärnbränslehantering AB.

SKB, 2021. Äspö Hard Rock Laboratory Annual Report 2020. SKB TR-21-10, Svensk Kärnbränslehantering AB.

Svemar C, Johannesson L-E, Grahm P, Svensson D, Kristensson O, Lönnqvist M, Nilsson U, 2016. Prototype Repository. Opening and retrieval of outer section of Prototype Repository at Äspö Hard Rock Laboratory. Summary report. SKB TR-13-22, Svensk Kärnbränslehantering AB.

Wallis I, Idiart A, Dohrmann R, Post V, 2016. Reactive transport modelling of groundwater-bentonite interaction: Effects on exchangeable cations in an alternative buffer material in-situ test. Applied Geochemistry, 73, 59–69.

Wersin P, Kiczka M, Rosch D, 2014. Safety Case for the Disposal of Spent Nuclear Fuel at Olkiluoto. Radionuclide Solubility Limits and Migration Parameters for the Canister and Buffer. POSIVA Report 2012-39, Posiva, Finland.